Detection of bacteria through taste receptors primes the cellular immune response

Alix Najera Mazariegos[1], Gérard Manière[3], Léo Sillon[2], Romane Milleville[4], Martine Berthelot-Grosjean[3], Enisa Aruçi[2], Darius Camp[1], George Alves[3], Rhea Kaul[1], Carla Jane Duval[1], Isabelle Chauvel[2], Julien Royet[4], Yaël Grosjean[3], Pierre-Yves Musso[1,2]*•, Guy Tanentzapf [1]*•

1: Department of Cellular and Physiological Sciences, University of British Columbia, Vancouver, Canada.
2: TPI team, Centre des Sciences du Goût et de l'Alimentation, AgroSup Dijon, CNRS, INRAe, Université Bourgogne Europe, F-21000 Dijon, France.
3 : PERSING team, Centre des Sciences du Goût et de l'Alimentation, AgroSup Dijon, CNRS, INRAe, Université de Bourgogne Europe, F-21000 Dijon, France.
4: Aix-Marseille Université, CNRS, IBDM, Marseille, France.

•: Co-senior authors
*: corresponding authors
Correspondence: tanentz@mail.ubc.ca; Pierre-Yves.Musso@ube.fr

SUMMARY
Animals use their sensory system to detect cues in their external environment, then communicate, process, and integrate these cues through the nervous system in order to elicit a specific response. Taste is an important cue used by animals to explore their external environment and can modulate various aspects of animal behavior and physiology. A major ongoing challenge for animals is to detect and respond to the presence of a variety of microbes in their environment. However, to date, the links between the sensory system and the response to pathogenic threats remain poorly understood. Here we show that *Drosophila* larvae use their taste system to detect bacterial peptidoglycans in their environment and respond by modulating the activity of their cellular immune system. We show that specific PeptidoGlycan Receptor Proteins (PGRPs) act in aversive taste neurons, via a non-canonical IMmune Deficiency (IMD) pathway. These PGRPs mediate signaling in taste neurons and control immune cells production in the larval hematopoietic organ, the lymph gland. Taste-mediated sensing of bacteria in larvae primes the immune system, and improves survival after infection in adult flies. These results demonstrate that sensory inputs such as taste play an important role in protecting animals from bacterial infection by providing a powerful adaptive response to potential pathogens. Overall, our findings add to the growing list of examples of crosstalk between the nervous and immune systems and provide novel and important mechanisms for linking them.

INTRODUCTION
Animal homeostasis requires constant monitoring of the environment so that animals can adapt and respond to external cues. Key to animal survival is their ability to detect the presence of both the nutrients they need to survive and possible pathogens and toxins in the

environment. The detection and analysis of chemical cues through the senses of smell and taste is an important method used by animals to monitor their environment. Smell and taste are used by animals to communicate, detect food, analyze food quality, and drive ingestion. In humans, for example, the detection of food decomposition through taste and smell drives avoidance or rejection behavior [1], whereas food-associated odor and taste drive attraction behavior towards the food source [2]. Although such behaviors vary widely among animals and are context specific, the general regulatory principles are conserved. This is exemplified by taste modalities that are well conserved in animals ranging from humans to *Drosophila* [3].

After ingestion, food is digested and evaluated through post-ingestive processes [4,5]. A high energy content will assign a positive value to the food, which is regulated by neurohormonal pathways such as insulin signaling [6]; whereas a post-ingestive illness will assign a negative value to the food, and lead to a biological response aimed at reestablishing homeostasis [7–9]. In particular, toxic food-borne compounds can induce a stereotyped immune response to restore homeostasis. Pathogen recognition can trigger a variety of immune-mediated responses to either remove or destroy the threat [10]. Although immune responses are generally the result of an infection, *i.e.* the entry of pathogens into the organism, pathogen-associated olfactory cues can act at a distance to control infection-avoidance behavior, without direct contact between the animal and the pathogen [11]. However, little is known about whether or how the detection of sensory cues can indicate a pathogenic threat, prime the immune response, or prepare the organism for the possibility of an infectious challenge.

Drosophila provides a powerful genetically tractable model system for studying immunity. Similar to humans, *Drosophila* displays humoral and cellular immunity [10]. Humoral immunity drives the regulated expression of genes encoding antimicrobial peptides (AMPs) which directly kill infecting microbes by disrupting their membranes and internal functions. Cellular immunity involves the recruitment of specialized immune blood cells, called hemocytes in invertebrates, to sites of infection and wounds. Hemocytes interact directly with invading microbial cells, phagocytosing or killing them. Cellular immune responses are initiated immediately upon recognition of infection and significantly reduce the number of invading microbes [10].

The site of immune cell production in the Drosophila larval stages is a specialized organ called the **L**ymph **G**land (LG), located in the anterior region of the larvae adjacent to the heart tube. Several factors make the *Drosophila* larvae a useful model for studying hematopoiesis, including its mechanistic conservation with vertebrate blood development, the wide availability of genetic tools and reagents, and its accessibility for imaging [12]. During fly hematopoiesis, a distinct population of blood progenitors gives rise to blood cells that serve as the fly's cellular immune system. Drosophila blood progenitors, known as prohemocytes, exhibit many stem-cell-like properties and their behavior is controlled by a small population of specialized cells that act as a hematopoietic niche, the Posterior Signaling Centre (PSC) [13–16]. Prohemocytes can give rise to plasmatocytes, lamellocytes, and crystal cells, three highly differentiated blood cell types that have unique functions and roles in the cellular immune response in flies [17]. Specifically, plasmatocytes, that represent more than 90% of hemocytes,

are the functional equivalent of human macrophages and engulf and consume microbes and dead host cells; crystal cells drive melanization for wound repair; while lamellocytes are expressed only in response to parasitic wasp infestation. The *Drosophila* immune system is activated by direct contact of immune cells with bacterial pathogens. This response is driven by toll-like and peptidoglycan receptors that recognize a variety of bacteria by direct binding but can also be modulated by environmental cues [10,11,18,19]. For example, anosmic flies, which are unable to smell, exhibit increased blood cell differentiation, suggesting that chemically based sensory inputs may regulate the cellular immune response [11].

There is considerable conservation in how animals detect and respond to taste. Sensory cells in both flies and mammals express gustatory receptors that are specialized in the detection of specific tastants, the activation of which drives specific behaviors, exemplified by the appetitive response to sweet taste and the aversive response to bitter taste [3]. Taste modalities are generally divided into 5 families: Sweet, Bitter, Umami, Sour, and Salt. However, the ongoing discovery of new taste sensory pathways such as bacteria sensing or fatty acid sensing suggest an even greater complexity to the sense of taste. There are multiple examples of taste controlling behavior in flies. For example, taste-mediated detection of the chemical signature of Gram-negative bacteria in adult flies, and subsequent activation of the immune-specific IMD pathway in the taste sensory organs, induces a refusal to lay eggs in contaminated areas and a rejection of contaminated-food [20,21]. Another example of the complex behavior controlled by taste modalities in flies is the observation that sweet taste acts as a predictor of metabolic value and consequently regulates feeding [5,9,22–24]. The question arises as to whether the pathways that act downstream of taste go beyond modifying behavior and alter other aspects of animal homeostasis in response to the detection of the chemical signature of potentially pathogenic bacteria.

Here we show that, in *Drosophila*, the detection of bacteria-derived pathogen-associated molecular patterns (PAMPs) via taste regulates homeostasis in an unexpected way, by modulating hematopoiesis. Specifically, we show that the genetic silencing of the taste-sensing peripheral neurons induces an increase in immune plasmatocyte production in the LG. The neuronal population underlying this change is shown to be involved in aversive bitter taste, which also drives the aversive response to food. RNAi-mediated gene knockdown shows that the well-established bitter taste receptor Gr66a is not involved in the changes in immune homeostasis. However, we find out that aversive taste neurons detect Gram-negative bacteria via the peptidoglycan receptor PGRP-LC which then activates the a non-canonical IMD pathway to suppress neural activity that promotes plasmatocyte differentiation in the LG. In addition, suppression of the ability to sense Gram-negative bacteria reduces plasmatocyte differentiation while overactivation of the IMD pathway within aversive taste neurons strongly promotes plasmatocyte differentiation and improves the survival of adult flies following infection. This finding demonstrates that the chemical sense of taste plays a role in the homeostatic regulation of immunity and its adaptation to pathogens throughout life.

RESULTS

Taste modulates hematopoiesis

To determine whether taste regulates hematopoiesis, we monitored blood cell differentiation and blood progenitor maintenance in third instar larval LGs whose most peripheral taste neurons were silenced by expression of the tetanus transgene under the control of the *poxn-Gal4* driver (*poxn-Gal4 > UAS-tnt*). By staining for the mature blood cell marker P1, we found that silencing peripheral taste sensory neurons resulted in an increase in the number of differentiated blood cells compared to controls. (Fig. 1a-b and Extended Data Fig. 1a-c). Using *UAS-GFP* we confirmed that *poxn-Gal4* did not drive expression in any region of the LG supporting the idea that it was indeed its ability to silence taste sensory organs that led to increased blood cell differentiation (Extended Data Fig. 1d-d'''). Overall, these data suggested that taste modulates hematopoiesis in the fly.

Aversive taste neurons modulate plasmatocyte differentiation

The *poxn-Gal4* driver is expressed in a broad population of neurons that sense the full spectrum of taste modalities (sweet, bitter, sour, salt, umami) [25,26]. Different taste modalities have the ability to independently drive different behavioral responses in *Drosophila* based on the information they convey. For example, sweet taste drives appetitive behavior by indicating high caloric value, whereas bitter taste drives food rejection behavior by indicating the possible presence of toxins [27]. An additional level of complexity is that taste modalities, such as salt or sour, can drive different behaviors depending on the concentration of the tastant, *e.g.,* low salt drives attraction while high salt drives repulsion [28–30]. To gain insight into why neural silencing of most taste sensory neurons using *poxn-Gal4* affects hematopoiesis, we sought to identify the specific taste neurons that mediated this response. To this end, we silenced neurons targeting specific taste modalities and measured their impact on hematopoiesis. First, we used the *IR94e-Gal4* (*VT046252-Gal4*) to silence neurons responsible for sensing low salt and amino acids (*IR94e-Gal4 > UAS-tnt*, [28,30]); and the $IR7C^{Gal4}$ driver to silence taste neurons that mediate high salt sensing ($IR7c^{Gal4}$ *> UAS-tnt*, [29]). These experiments showed that silencing neurons for amino acid and high salt sensing did not affect hematopoiesis (Extended Data Fig. 1e-n'''). Second, we used the *Gr66-Gal4* driver, to silence peripheral bitter-activated aversive taste neurons in both larvae and adults (*Gr66a-Gal4 > UAS-tnt)* [31–33]. We observed that silencing of aversive taste neurons resulted in an increase in hematopoiesis compared to controls (Fig. 1c, d; Extended Data Fig. 1o-r'''). Interestingly, no modification of crystal cells nor lamellocytes was observed (Fig. 1e, f; Extended Data Fig. 1s-w). As before, we confirmed that this effect is mediated by expression in sensory neurons as we did not observe any *Gr66a-Gal4* driven expression in the LG or the nearby digestive tract (Extended Data Fig. 1r-r''', and Extended Data Fig. 1zb), but we did see strong expression in the peripheral taste organs (Extended Data Fig. 1zb). Interestingly, the increased plasmatocyte differentiation is not due to a metabolic difference since silencing Gr66a aversive taste neurons does not affect feeding (Fig. 1g-i; Extended Data Fig. 1x). Taken together, these data strongly suggest that the impairment of peripheral aversive taste neurons leads to a specific increase in plasmatocyte differentiation in the LG without affecting feeding.

Activation of aversive taste neurons inhibits plasmatocyte differentiation

Since suppressing the activity of aversive taste neurons caused an increase in plasmatocyte differentiation in the LG, we asked whether the opposite treatment, consisting of activating these neurons using optogenetic tools, would modulate plasmatocyte differentiation. Specifically, we expressed the light-activated optogenetic transgene CsChrimson using *Gr66a-Gal4*. When larvae are fed with the cofactor all-trans retinal and exposed to red light CsChrimson causes neural activation [34] (Fig. 2a and 2c). We observed that activating Gr66a-expressing neurons (see materials and methods) promoted a reduction in plasmatocyte differentiation (Fig. 2b and 2d, and Extended Data Fig. 2). These data demonstrate that the activity of Gr66a-expressing neurons is inversely correlated with plasmatocyte differentiation. When their activity was low, the level of differentiation level was high; conversely, when their activity was high, the level of plasmatocyte differentiation was low (Fig. 2e).

Detection of Gram-negative bacteria-derived peptidoglycans by Gr66a neurons inhibits their activity

Our data implicate aversive taste neurons expressing the Gr66a taste receptor in the regulation of plasmatocyte differentiation. However, this does not necessarily mean that the Gr66a gustatory receptor directly mediates this effect. To test whether this was the case we used RNAi to knock down the expression of the bitter-sensing gustatory receptor Gr66a [31–33] in the *Gr66a-Gal4* neural population (Extended Data Fig. 3a-d). We found that the knockdown of the Gr66a receptor did not alter plasmatocyte differentiation, as it was similar to that observed in controls (Extended Data Fig. 3a-d). This finding suggests that the modulation of plasmatocyte differentiation by Gr66a-expressing neurons was not due to simple bitter receptor sensing activity but was likely due to another taste modality. Consistent with this idea, previous work has shown that Gr66a-expressing neurons have the ability to detect other food derived compounds [35–37]. We then investigated whether these alternative taste modalities might be involved in the regulation of plasmatocyte differentiation in the fly larvae.

First, we noted that previous work implicated Gr66a-expressing neurons in a behavioral rejection response induced by lipopolysaccharides (LPS), bacterial endotoxins that are known to activate the innate immune response [35]. Specifically, LPS has been detected through a chemosensory cation channel, dTRPA1, that functions in Gr66a-expressing neurons [35,36]. To test whether LPS detection by Gr66a-expressing bitter taste neurons was responsible for modulating of plasmatocyte differentiation, we used RNAi to knock down TRPA1 using *Gr66-Gal4* (Extended Data Fig. 3a-d). We found that TRPA1 knockdown did not alter plasmatocyte differentiation which was similar to that observed in controls (Extended Data Fig. 3a-d). These data argue against the hypothesis that LPS sensing by Gr66a neurons underlies their ability to modulate plasmatocyte differentiation.

Second, a recent study demonstrated that a subpopulation of Gr66a-expressing neurons in adult flies is capable of sensing bacteria-derived peptidoglycans (PGN) through peptidoglycan recognition proteins (PGRPs). Specifically, PGRP-mediated activation of Gr66a-expressing neurons resulted in reduced oviposition and feeding behavior in adult flies through a mechanism involving signaling through the IMmune-Deficiency (IMD) pathway, a

canonical immune signaling pathway in flies [20]. Finaly, in adult flies, Gr66a-expressing neurons display calcium signaling activity in response to the presence of PGN or *E. coli* in *in-vivo* experiments [20].

This suggested that a subset of Gr66a-expressing neurons detect bacteria-derived PGNs, and we sought to test this directly by visualizing neuronal activity in larval taste neurons. We adapted a method previously used to analyze neuronal activity in adult flies following the addition of Gram-negative bacteria-derived PGNs [20]. This technique uses the reporter transgene *UAS-GCaMP6s* to monitor calcium signaling activity specifically in Gr66a-expressing neurons before and after the addition of different tastants. As a control, using bitter tasting quinine, we confirmed that Gr66a-expressing neurons show increased activity following bitter taste detection (Fig. 3a-b; Extended Data Fig. 4a, and Extended Data Movie 1). In contrast, the addition of PGNs from Gram-negative bacteria did not result in an increase in calcium signaling activity in Gr66a-expressing neurons (Fig. 4b). Importantly, experiments in which larvae were pre-incubated with PGNs and stimulated with quinine and PGNs revealed a dose-dependent inhibitory effect of PGNs on bitter sensing in Gr66a-expressing neurons (Fig. 3c, and Extended Data Fig. 4b, and Extended Data Movie 2). The specificity of this effect was demonstrated by knocking down the PGN receptor PGRP-LC in *Gr66a-Gal4* neurons, which abolished the inhibitory effect of PGNs on the response to quinine (Fig. 3d, and Extended Data Fig. 4c, and Extended Data Movie 3). Taken together, these results demonstrated that sensing of Gram-negative bacteria-derived PGNs by Gr66a-expressing neurons through the PGRP-LC receptor led to the inhibition of neural activity.

Modulation of plasmatocyte differentiation by Gr66a-expressing neurons is mediated by PeptidoGlycan Receptor Proteins and a non-canonical Immune Deficiency pathway. Since Gram-negative, bacteria-derived, PGNs are recognized by members of the PeptidoGlycan family of transmembrane receptor proteins [19,38] we asked whether these receptors also control plasmatocyte differentiation. Notably, previous studies have shown that PGRPs signal through the IMD pathway, which is required for antibacterial response of flies [10,19,38]. Although there are several PGRPs in flies that have distinct roles, the ability to signal through the IMD pathway is a shared feature. For example, PGRP-LC detects bacteria by binding to PGNs, and acts as a key regulator of the IMD pathway during the systemic immune response in the fat body [10]. Moreover, PGRP-LA and PGRP-LF, neither of which is known to directly bind PGNs, act as positive and negative regulator of the IMD pathway, respectively [10,39–41]. Binding of PGNs to the PGRP-LC receptor regulates several protein components of the IMD signaling pathway including IMD, Fadd, dredd, and controls the nuclear localization of the NF-kB transcription factor Relish [10]. To determine whether Gr66a-expressing neurons sense PGNs through PGRPs and the IMD pathway, we used RNAi-mediated knockdown for various PGRPs and IMD components (Fig. 4a). We found that knocking-down the PGRP-LC receptor specifically in Gr66a neurons resulted in a reduced blood cell differentiation (Fig. 4, and Extended Data Fig. 5a-c). In addition, knockdown of the positive PGRP-LC regulator PGRP-LA also resulted in plasmatocyte differentiation, whereas knockdown of the negative PGRP-LC regulator PGRP-LF resulted in increased plasmatocyte differentiation (Fig. 4, and Extended Data Fig. 5a-c) as well as an increased

inhibitory effect of PGN to the response to quinine (Extended Data Fig. 4d). Knockdown of downstream components of the IMD pathway such as Dredd and Fadd also led to a decreased plasmatocyte differentiation (Extended Data Fig. 5d-j). Interestingly, knockdown of the transcription factor Relish using two different RNAi lines did not impact plasmatocyte differentiation, suggesting that the IMD signaling pathway in Gr66a neurons is non-canonical (Fig. 4, and Extended Data Fig. 5a-c). Knocking-down Spätzle and cactus, two essential components of the Toll pathway did not impact plasmatocyte differentiation (Extended Data Fig. 5k-n). A previous study demonstrated a functional link between the IMD pathway and the JNK pathway [39]. Interestingly, knocking-down two kinases of the JNK pathway (basket and Hep) led to a decrease of plasmatocyte differentiation (Extended Data Fig. 5k-n). Finally, modulation of the IMD pathway in Gr66a neurons did not impact larval feeding (Extended Data Fig. 5o, p). These results demonstrated that plasmatocyte differentiation was controlled by a non-canonical IMD-based pathway that was active in Gr66a-expressing taste neurons.

Detection of Gram-negative bacteria through PGRP-LC regulates blood cell differentiation

Our results were consistent with a model in which Gr66a-expressing neurons detect PGNs, leading to activation of the IMD pathway and consequent modulation of plasmatocyte differentiation. To directly relate these observations to bacterial detection under physiological conditions, we asked whether Gr66a-expressing neurons detected Gram-negative bacteria and whether this resulted in increased immune cell production in flies. To address this question, we raised larvae in an antibiotic enriched (ATB) media (germ-free environment; see materials and methods), and then exposed them to a Gram-negative bacteria, *E. coli* (Fig. 5a; see materials and methods). Consistent with previous observations, we found that exposure to *E. coli* was sufficient to induce an increase in plasmatocyte differentiation (Fig. 5b, and Extended Data Fig. 6). We found that knockdown of PGRP-LC in Gr66a-expressing neurons resulted in decreased plasmatocyte differentiation both in the presence and in the absence of bacteria, consistent with its basal activity even under the unexposed conditions (Fig. 5b, and Extended Data Fig. 6). Importantly, knockdown of the inhibitory PGRP-LF, which is expected to enhance PGRP-LC function, resulted in an increase in plasmatocyte differentiation but only in the presence of bacteria (Fig. 5b, and Extended Data Fig. 6). This result suggests that PGRP-LF acted as an inhibitor of PGRP-LC but only in the presence of bacteria. Taken together, these results show that, in aversive taste neurons, modulation of PGRP-LC activity controlled plasmatocyte differentiation (Fig. 5c, and Extended Data Fig. 6).

Sensory detection of Gram-negative bacteria primes the immune system

Our results were consistent with a model in which sensory detection of Gram-negative bacteria promotes hematopoiesis and, in particular, plasmatocyte production. Plasmatocytes play a critical role in bacterial defense, and flies lacking plasmatocytes show susceptibility to several microorganisms and reduced survival following infection [42]. We asked whether increased plasmatocyte differentiation following sensory detection of an exposure to *E. coli* would confer improved resistance to bacterial infection. To this end, we reared larvae in germ-free condition (see materials and methods) and exposed them briefly to *E. coli*. After

pre-exposure, we returned the larvae to antibiotic-containing vials to continue development. We collected the adults that emerged, infected them with *Pseudomonas entomophila* by puncture, and monitored their survival over time (Fig. 6a). The the pre-exposure period was deliberately kept short so as to avoid inducing a large scale systemic immune response, evidenced by the rather small increase (of about 6%) in plasmatocyte numbers in these larvae (Fig. 6). Consequently, we found that infected adults pre-exposed to *E. coli* as larva did not fare any better than infected adults that were not pre-exposed (Fig. 6b, and Extended Data Fig. 6a,c-e). Similarly, the small reduction in plasmatocyte numbers caused by PGRC-LC knockdown in Gr66a-expressing neurons in larvae (~15%, Fig. 5) did not impact adult survival (Extended Data Fig. 7a and f). In contrast, larvae in which increased the sensitivity to taste inputs in Gr66a-expressing neurons by knocking down the IMD pathway inhibitor PGRP-LF, showed a larger increase, of up to 31% more plasmatocytes, following pre-exposure. Importantly, larval pre-exposure of these sensitized PGRP-LF knockdown larva improved survival following adult infection (Fig. 6, 7b, and Extended Data Fig. 7a and b). These data suggest that larval exposure to bacteria which induced a sufficiently large taste-mediated increase in plasmatocyte numbers, conferred increased resistance to infection at the adult stage (Fig. 7C).

DISCUSSION

Here, we provide evidence that taste modulates plasmatocyte differentiation by regulating the activity of taste sensory neurons. Specifically, by targeting neuronal populations associated with specific taste modalities, we found that the Gr66a-expressing neuronal population, canonically involved in aversive taste perception, also plays a role in modulating plasmatocyte differentiation. Furthermore, we showed that acute optogenetic activation of Gr66a-expressing neurons was sufficient to suppress plasmatocyte production, suggesting that acute taste perception directly controls plasmatocyte differentiation. Using calcium imaging experiments, we found that taste stimulation of living larvae with peptidoglycans (PGNs) from Gram-negative bacteria inhibited the activity of Gr66a-expressing neurons. This effect was rescued by knocking out PGRP-LC in Gr66a-expressing neurons, a receptor that detects Gram-negative PGNs, showing that Gr66a-expressing neurons detect PGNs. Using RNAi, we showed that silencing PGRP-LC and the downstream IMD signaling pathway in Gr66a-expressing neurons modulated plasmatocyte differentiation. Furthermore, short-term exposure to Gram-negative bacteria-contaminated medium increased plasmatocyte differentiation through activation of the IMD pathway in Gr66a taste sensory neurons. Finally, we showed that taste-induced activation of hematopoiesis confers a survival advantage upon infection in adult flies. Based on these findings, we propose a mechanism that allows *Drosophila* larvae to detect bacteria by taste and, in response, modulate plasmatocyte differentiation in anticipation of an increased risk of infection.

Taste receptors can trigger the immune response via a neural pathway

The detection of pathogens by cells expressing taste receptors is a well-known phenomenon in mammals. For example, cells localized in the solitary chemosensory cells of the epithelial mucosa, the brush cells of the respiratory tract, as well as the tuft cells of the digestive system express various taste receptors and detect pathogens [43]. Upon detection of pathogens, these

cells locally release antimicrobial peptides or interleukins, which are components of the humoral immune system [43]. Importantly, while typical taste receptor cells located in the taste buds send receptor-derived information to the brain, to reports of taste-derived pathogen detection have so far only been shown to act independently of neural pathways and act locally [43]. In our study, Gr66a-expressing PGN-sensory neurons are located in sensory organs whose organization is similar to that of mammalian taste buds [3]. These sensory neurons send axonal projections to the brain and transmit sensory information to higher brain structures [44–47]. This suggests that, at least in some contexts, receptors that taste bacteria may signal via an intermediate neural network rather than via local secretion.
At present, it is not clear how neuronal signals are transmitted from the brain to the LG but there are several obvious candidates. Previous research has shown that fly hematopoiesis is under the control of multiple signals originating in the brain [10,11,48,49]. For example, both Drosophila insulin like proteins (DILPS), produced in the brain and the neurotransmitter GABA, regulate hematopoiesis in the LG [18,48,50]. In addition, the serotonin receptor 5-hydroxytryptamine 1B (5-HT1B) is expressed in the LG [49]. Our future work will aim to identify which of these signals are specifically involved in signaling downstream of taste receptors.

Different sensory modalities drive different hematopoietic fates
Previous studies have reported that olfaction can regulate hematopoietic progenitor maintenance [11,48,51]. Specifically, these experiments showed that odor-mediated cues in food induce neuronal signaling that is essential for the maintenance of blood progenitors [11]. In addition, subsequent work demonstrated that olfaction influences hematopoiesis by promoting lamellocyte production in anticipation of parasitic wasp infestation [11,51]. We found that exposure to a taste indicating the presence of Gram-negative bacteria specifically promotes plasmatocyte differentiation. Thus, different sensory modalities may act to promote the production of specific types of blood cells to ensure that animals can respond to different challenges. As *Drosophila* encounters a variety of other pathogens in its environment, such as Gram-positive bacteria and fungi, we hypothesize that there are likely unique sensory modalities that also detect and respond to these pathogens as well and drive an appropriate anticipatory immune response.

A link between the activity of Gr66a-expressing neurons activity and plasmatocyte differentiation
Our results suggest a connection between the activity of Gr66a-expressing neurons and plasmatocyte differentiation. Reducing Gr66a-expressing activity promoted plasmatocyte differentiation while increasing their activity resulted in decreased blood cell differentiation. Gr66a-expressing neurons produce a variety of receptors activated by particular tastants: Gr66a (bitter compounds), Ir7c (high salt); Ir25a (metal ions, carboxilic acids, amino acids); Ir7a (metal ions, carboxylic acids), Alka (alkaline solutions); TrPA1 (lipopolysaccharides); carboxylic acids; fatty acids, rhodopsins 1, 4, and 7 (aristocolic acids) [30,35,37,52–59]. A knockdown of the Gr66a receptor removes the ability of Gr66a-expressing neurons to sense bitter taste, but should not impact these other pathways. In comparison, silencing neural activity in Gr66a-expressing neurons activity would suppress inputs from alternatives

pathways. We can assume that larvae crawling in food are exposed to diverse and constant taste stimulation. Based on this, we can envision two non-mutually exclusive scenarios that would result in blood cell differentiation: first, that differentiation is induced whenever the general activity of Gr66a-expressing neurons falls below a certain threshold, or second, that differentiation is induced whenever the inhibition of specific taste pathways in Gr66a-expressing neurons occurs. We provide direct evidence for this second scenario as exposure to PGN inhibits the activity of Gr66a expressing neurons and promotes blood differentiation.

Potential impact of taste-mediated bacterial sensing on feeding

It is known that silencing neurons expressing the Gr66a receptor in larvae does not affect the preference for sweet food but impairs the sensing of bitter compounds which innately trigger food rejection [60,61]. Indeed, impairing Gr66a neurons did not affect feeding on standard food media nor yeast extract. Our imaging data shows that the detection of bacteria-derived PGN inhibits the activity of bitter-sensing neurons, meaning that larvae should be less likely to reject a bitter-tasting food if it is contaminated with bacteria. In contrast, in adult flies the detection of bacterial PGNs induces an activation of the bitter-sensing neurons which is expected to lead to food avoidance [20]. In addition, recent work showed that the aversive response to *E. coli*-derived PGNs in the adult requires priming. Similarly, increased calcium signaling observed in a subset of neurons following exposure to *E. coli-derived* PGNs also required priming from Gr66a-expressing neurons. This means that flies raised conventionally will react aversively to PGNs, while flies raised in axenic condition may not display any particular reaction to them [21]. This raises the question of why fly larvae evolved to have a taste response that favors the consumption of bacterially-contaminated food. We can hypothesize that it may be beneficial for larvae to consume bacterially contaminated food in order to build up their cellular immune system and their microbiota, which, according to our experiments, may confer an advantage that can last until adulthood.

Taste-mediated recognition of bacteria primes adult immunity

Of the two branches of the immune system, innate and adaptive immunity, it is adaptive immunity that has long been associated with immunological memory [62]. However, a growing body of evidence suggests that immune memory is not restricted to the adaptive branch of the immune system [63,64]. In our study, we present evidence that the perception of PGNs derived from Gram-negative bacteria leads to the activation of the IMD pathway in taste sensory neurons, resulting in increased plasmatocyte differentiation. Importantly, larvae with a sufficiently large increase in plasmatocyte numbers show increased resistance to infection in adulthood. Thus, prior exposure to bacteria may promote resistance during a subsequent encounter with bacteria later in life, a phenomenon that at least superficially resembles immune priming and immune memory [64]. Previous studies have performed priming by infecting adult flies either by puncture or by ingestion. This induces both cellular and humoral responses. Our study demonstrates that priming can occur without the features associated with full-blown infection. Indeed, the sensory detection of a cue predictive of infection is sufficient to prime the immune system, a phenomenon we propose to call Taste-Primed Immunity (TPI). In contrast to previous studies of immune priming in flies, which have been conducted in adult stages and mostly focus on the humoral immune response, TPI

occurs at larval stages and has unique features. Specifically, TPI directly modulates the cellular immune response in larvae by promoting plasmatocytes differentiation. Since up to 90% of the circulating plasmatocytes in adults are derived from larval hematopoiesis [65,66], an increase in plasmatocyte production in the larvae would be predicted to confer increased immune resistance that persists into adulthood.

STAR METHODS

Drosophila melanogaster

Fly stocks were raised on standard food at 25C and 70% relative humidity under a 12-hour light/12-hour dark cycle. For neuronal silencing experiments, we used *UAS-tnt*. For neuronal activation experiments, we used *20XUAS-IVS-CsChrimson.mVenus* (Bloomington #55135). Global peripheral taste sensory neuron expression was driven using *poxn-Gal4* [25]. High salt taste sensory neuron expression was driven by *IR7c-Gal4* [29]. Low salt taste sensory neuron expression was driven by *IR94e-Gal4* (*VT046252-Gal4*) [28,30]. Bitter taste sensory neuron expression was driven by *Gr66a-Gal4* [32]. For staining experiments, we used *40XUAS-IVS-mCD8::GFP* (Bloomington#32195), For imaging experiments, we used the *20XUAS-IVS-GCaMP6s* (Bloomington #42746). For RNAi experiments, we used RNAi against Gr66a (Bloomington #31284), TrpA1 (Bloomington #66905), PGRP-LC (VDRC #101636KK), PGRP-LA (VDRC #102277KK), PGRP-LF (VDRC #108313KK), Dredd (VDRC #104726KK), Relish (VDRC #108469KK for RNAi1 and 49413GD for RNAi2), PGRP-LB (Bloomington #67236), PGRP-LD (Bloomington #34892), PGRP-LE (Bloomington #60038), Fadd (Bloomington #34813), PGRP-SB2 (Bloomington #56982), PGRP-SB1 (Bloomington #56983), PGRP-SC1b (Bloomington #67249), PGRP-SC2 (Bloomington #56315), bsk (Bloomington #35594), hep (Bloomington #28710), spz (Bloomington #28538), cactus (Bloomington #37484). Controls for RNAi experiments (Bloomington #35784; VDRC #60000TK).

Embryo sterilization

Embryo sterilization was performed as previously [21]. Three petri dishes are filled with 2.6% bleach, 70% ethanol (Ethanol 96° RPE Carlo Erba Ref 414638) and autoclaved purified distilled water respectively. The embryos are collected by filling the tube in which oviposition occurred with PBS and using a small brush to gently detach them from the flies' food. A 40µm cell strainer is used to collect the embryos. The cell strainer with the embryos is then dipped into: bleach 2.6% for 5 minutes, ethanol 70% for 1 minute, purified water for 1 minute, ethanol 70% for 1 minute, purified water for 1 minute. The brush used to collect the embryos is sterilized in 2.6% bleach for ten minutes, rinsed and then used to transfer the sterile embryos on antibiotic enriched media.

Larval exposure protocol

Early third instar larvae from sterile embryos were placed in petri-dish containing LB media (non-exposed group) or in petri-dish containing LB media contaminated with *E. coli* for thirty

minutes and then placed on petri-dish containing LB media for two hours and a half until dissection dissection (exposed group).

Larval feeding protocol

We used a previously published protocol from Bhatt & Neckameyer [67]. Third instar larvae were collected and transferred to the center of either an agar-filled plate overlaid with 5 ml of 2% activated baker's yeast solution, or to the center of a standard-food plate. The rate of mouth hook contractions directly correlates with the amount of food ingested. The larvae were acclimated for 30 sec. then observation and recording of the number of mouth hook contractions for a period of 1 min were performed. n = 30 for each genotype.

Dye ingestion protocol

Food-intake assays were performed using adapted protocol [68]. L3 Larvae were starved for 4 hours at 25°C on 1% agarose petri dishes as a water source to keep the inside of the container humidified. Behavioural tests used active yeast as food source. A blue food dye (Erioglaucine Disodium Salt, Sigma 861146) was added to the yeast at a 2:1 ratio. Starved larvae were carefully transferred into petri dishes with dyed yeast to start the feeding process for one hour. Larvae were homogenized in 200 µl PBS buffer in 1.5 mL Eppendorf tubes with a tungsten bead, and grinded 30s at 30 Hz (3 times). Products were centrifuged twice (10 000 r.p.m.) for 10 min to clear the debris. After centrifugation, the absorbance of the supernatant was measured at 630 nm (A630). The background absorbance for supernatants from flies fed with regular food was subtracted from the absorbance of the supernatant from blue food-fed flies. The net absorbance reflected the amount of food ingested. A n of 1 correspond to 10 larvae.

Dissections and Immunohistochemistry

Third instar larvae were collected and prepared for lymph gland dissection in cold 1% phosphate buffered saline (PBS) and fixed in 4% paraformaldehyde (PFA) for 15 minutes, then washed two times for 5 minutes with 0.1% PBST (PBS with 0.1% Triton-X [ThermoFisher Scientific BP151100]). The blocking step was done for 15 minutes using 16% Normal Goat Serum (NGS). Samples were then incubated overnight at 4ºC in a 1:100 dilution of anti-P1 (NimC P1 a+b) in 0.1% PBST primary antibody (gift from Dr. Istvan Ando, Hungarian Academy of Sciences, Hungary). After overnight incubation, the samples were washed twice for 5 minutes using 0.1% PBST and then blocked for 15 minutes with NGS. Secondary antibody incubation of the samples was done for 2 hours at room temperature using a solution of donkey anti-mouse cy3 (1:400, Code: 715-165- 150, RRID: AB_2340813, Jackson Immunoresearchlaboratories) and TO-PRO diluted in 0.1% PBST, followed by a set of three, 5-minute washes with 0.1% PBST. LG samples were mounted in glass bottom mounting dishes using VECTASHIELD Antifade Mounting Medium with TO-PRO (H-1200, Vector Laboratories, RRID:AB2336790). For crystal cell and lamellocyte stainings, samples were incubated overnight at 4°C in a 1:50 primary antibody dilution of anti-Hnt (DSHB; 1G9-s) or a 1:25 dilution of anti-L1 (gift from Dr. Istvan Ando, Hungarian Academy of Sciences,

Hungary) respectively, with 0.1 % PBST. After incubation, the samples were washed twice for 5 minutes in 0.1% PBST and blocked for 15 min in Neat Goat Serum (NGS). Secondary antibody incubation was done for 2 hours at room temperature with a solution of donkey anti-mouse cy3 (1:400, Code: 715-165- 150, RRID: AB_2340813, Jackson Immunoresearchlaboratories) and TO-PRO diluted in 0.1% PBST, followed by three, 5-minute washes with 0.1% PBST."

Survival experiments

LB agar plates were seeded with 100 µL of an overnight *E. coli* culture and incubated overnight at 37°C. Wandering third instar larvae were placed for 30 minutes on LB agar plates coated or not with *E. coli* and then transferred onto LB only plates for 2h30. By batch of 20, larvae were transferred into vials containing fly food supplemented with antibiotics placed in 25°C incubators until fly hatching. Hatched 5-to-7-day old females were puncted with a tungsten needle dipped into an OD10 solution of *P. entomophila*.

Imaging

For Lymph gland imaging, after overnight incubation, mounted LG samples were imaged using an Olympus FV1000 inverted confocal microscope with a numerical aperture 1.30 UPLFLN with the 40x oil immersion lens. Laser lengths used for detection of staining were 559 nm for Cy3 and 635 nm for Cy5. LG images were taken along the z-axis, 3nm apart.

For neuron imaging, larvae were partly dissected in PBS, fixed in 4% paraformaldehyde for 45 min at room temperature (RT). Anterior part of the larvae and guts were then isolated by precise dissection. They were mounted in VECTASHIELD® mounting medium (H-1000, Vector Laboratories). Fluorescence was observed with a Leica TCS SP8 confocal microscope.

***In vivo* calcium imaging**

In vivo larval calcium imaging experiments were carried out on wandering third instar larvae. Larvae were immobilized in a small drop of distilled water placed between two plastic coverslips (22 mm x 22 mm, Agar Scientific). The two coverslips were held together to prevent movement of the anterior part of the larvae, using alligator clips attached to a support. Stimulation was performed manually using a pipette with gel loading tip by applying water, PGN (50µg to 100µg/mL) or quinine (10 mM) diluted in water through a hole made in the upper coverslip allowing the solutions to come into contact with the Terminal Organ (TO) of the larvae. In PGN preincubation experiments, larvae were preincubated with the indicated dilution of PGN for one or two minutes and a solution containing the appropriate dilution of PGN and 10mM quinine was applied. Gr66a neurons were recorded in the TO of heterozygous larvae (*GR66a-Gal4>UAS-GCaMP6s*) with a 10x dry objective. GCaMP6s was excited using a Lumencor diode light source at 482 nm ± 25. Emitted light was collected through a 505-530 nm band-pass filter. Images were collected every 500ms using a Hamamatsu/HPF-ORCA Flash 4.0 camera and processed using Leica MM AF 2.2.9. Each experiment consisted of a recording of 70-100 images before stimulation and 160 images after stimulation. Data were

analyzed as previously described[20] by using FIJI (https://fiji.sc/). For larvae fluorescence quantifications, a background fluorescence variation was calculated and subtracted to the fluorescence variation signal. For each image, ROIs were manually drawn on the left and right side and the signal intensity was quantified. These data were then manually inspected to exclude images with clear signs of drift and to select the side with the least variation in response. The initial intensity F_0 was calculated over 10 frames, 30 frames before the stimulus, and $\Delta F/F_0$ was expressed as a percentage. Peak $\Delta F/F_0$ was calculated as the average $\Delta F/F_0$ over 4 frames around the peak minus average $\Delta F/F_0$ over 4 frames immediately before the peak. Statistical differences in peak $\Delta F/F_0$ between species were assessed using the Mann–Whitney U test. For calcium imaging experiments, Peptidoglycan (PGN) was purchased from InvivoGen (PGN-EK, # tlfl-pgnek) and quinine from Sigma-Aldrich (# Q1125).

Optogenetics

The optogenetics experiments set up in this study were designed based on the protocol by Honjo *et al*, 2012[69]. Genetic crosses were set up to yield *Gr66a-Gal4 / UAS-Chrimson* and *PLB-Gal4 / UAS-Chrimson* lines. Larvae were kept in vials and growing in the dark as Chrimson is a photosensitive channel that might be deactivated due to light exposure. For both genotypes, two groups of larvae were made respectively. One group was fed fly food that contained 2.5 µL of 100 µM all-trans-retinal (Ret+), a cofactor of channelrhodopsin. The second group of larvae were fed food containing 2.5 µL of ethanol (Ret-). Ret+ and Ret- groups of larvae were subjected to one of two conditions, they were either exposed to three cycles of 15 minutes of red LED light (671 nm) with 15 minutes in between cycles where they were kept in the dark, or they were not exposed to LED light at all. To allow time for hemocyte differentiation LGs were dissected two hours after the last cycle.

Glucose and Glycogen Assay

For glucose and Glycogen assay, we adapted a previously published protocol [70] . 10 larvae L3 were collected in a pre-weighed 1.5 mL tubes and stored at -80°C until processed. Before starting the assay, we weighed the tubes containing the larvae as they come out of the freezer. Larvae were then homogenized using 3 x 2mm Zirconium oxide beads (Next Advance – ZROB20) in 200 µl PBS 1X with a tissue lyser (Qiagen) (3X1 min at 30hz). There were centrifuged (Eppendorf centrifuge 5430R) a first time for 10 min at 10000 rpm at 4°C. For each sample, 50 µL of homogenate were transferred to a 1.5mL eppendorf and heat treated at 70°C for 10 min. They were again centrifuged for 7 min at 10000 rpm at 4°C to precipitate cell debris. A glucose standard curve was prepared using Glucose standard (Sigma – G3285) for concentrations of 0 mg/ml, 0.02 mg/mL, 0.04 mg/mL, 0.08 mg/mL and 0.16 mg/mL and a Glycogen standard curve was prepared using Glycogen (Thermo Fisher Scientific, AM9510) for concentrations of 0 mg/ml, 0.02 mg/mL, 0.04 mg/mL, 0.08 mg/mL, 0.16 mg/mL and 0.24mg/mL. Glucose reagent was made by adding 20µL of o-Dianisidine (Sigma F5803) to 1 mL of GO reagent (Sigma, G3660). Glycogen reagent was made by adding 20 µL of Amyloglucosidase (Sigma, A7420) to 1 mL of GO reagent (Sigma, G3660) added with 20µL of o-Dianisidine (Sigma F5803). 30 µL of each standard curve concentration was added into a 96-well plate-reader plate. 6 µL of each sample and 24 µL of 1X PBS were loaded in duplicate

to the same 96-well plate-reader plate. 100 µl of Glucose reagent was added to 1 set of samples and the glucose standard curve, 100 µL of Glycogen reagent to the other set of samples and to the glycogen standard curve. Samples were incubated at 37°C for 60 minutes. 100 µl of 12N H2SO4 was added to every well. Absorbance was read at 540 nm (Labtech – SpectroStar Nano)

Statistical Analysis

Analysis of the images from stained LGs was carried out using a custom written MatLab script (**Ho et al, 2023; available through our lab's Github account https://github.com/Tanentzapf-Lab**). LGs were individually assessed to count P1-stained cells, total cell numbers based on nuclear staining and the ratio of P1-stained cells to to total cell count was determined. Statistical tests were performed using GraphPad Prism 6 software. Descriptions and results of each test are provided in the figure legends. Sample sizes are indicated in the figure legends. Biological replicates used different larvae. Data for all quantitative experiments were collected on at least three different days, and behavioral experiments were performed with larvae from at least two independent crosses.

ACKNOWLEDGEMENTS

We thank the members of the Tanentzapf lab, the TPI lab, the Persing lab and the J. Royet's lab for the comments on the manuscript. We thank M.D. Gordon for providing *Ir7c*^{Gal4} and *Ir94e-Gal4* (*VT046252-Gal4*) lines. We thank the Bloomington stock center and the Vienna Drosophila resource center for fly stocks. We thank Dr. Istvan Ando for P1 antibodies. We thank Leopold Kurz for his useful guidance.

This work was supported by: the Canadian Institutes of Health Research (Project Grant PJT-156277) to GT; by grants from Conseil Régional de Bourgogne- Franche Comté (PARI, ALIMENN grants) to GM; by the CNRS (to PYM, MBG and YG); by Atip-Avenir grant (CNRS Biology, to PYM); by the University of Burgundy Europe (GM and GA); by the GliSFCo grant (ERC, to YG), and Burgundy Council/FEDER (to YG); by the CNRS, ANR BACNEURODRO (ANR-17-CE16-0023-01), Equipe Fondation pour la Recherche Médicale (EQU201603007783) et l'Institut Universitaire de France to J.R. and by the ANR PepNeuron (ANR-21-CE16-0027) to J.R and YG.

AUTHOR CONTRIBUTIONS

P.Y.M. Conceptualization, Formal analysis, Validation, Investigation, Visualization, Methodology, Writing – original draft, Writing – review and editing; A.N.M. Validation, Investigation, Visualization; D.C. Validation, Investigation; M.B-G and Y.G. Validation, Investigation; G.M. Validation, Investigation; J.R. Validation, Investigation; G.T. Resources, Validation, Writing – original draft, Project administration, Writing – review and editing; R.K. analysis; G.A. Investigation, Visualization; R.M. Validation, Investigation; L.S. Validation, Investigation; E.A. Validation, Investigation; I.C. Validation, Investigation.

DECLARATION OF INTERESTS

The authors declare no competing interests.

INCLUSION AND DIVERSITY

We support inclusive, diverse, and equitable conduct of research.

LIST OF SUPPLEMENTARY MATERIALS

Materials and Methods
Supplementary Text
Extended Data Figs. 1 to 7
Extended Data Movie 1 to 3

DATA AVAILIABILITY

Data for this paper is available upon request.

REFERENCES

1. Wisman, A. & Shrira, I. The smell of death: evidence that putrescine elicits threat management mechanisms. *Front. Psychol.* **6**, 1274 (2015).
2. Boesveldt, S. & Graaf, K. de. The Differential Role of Smell and Taste For Eating Behavior. *Perception* **46**, 307–319 (2017).
3. Yarmolinsky, D. A., Zuker, C. S. & Ryba, N. J. P. Common sense about taste: from mammals to insects. *Cell* **139**, 234–244 (2009).
4. Sclafani, A. Post-ingestive positive controls of ingestive behavior. *Appetite* **36**, 79–83 (2001).
5. Musso, P.-Y., Lampin-Saint-Amaux, A., Tchenio, P. & Preat, T. Ingestion of artificial sweeteners leads to caloric frustration memory in Drosophila. *Nature communications* **8**, 1803 (2017).
6. Ratnaparkhi, A. & Sudhakaran, J. Neural pathways in nutrient sensing and insulin signaling. *Front. Physiol.* **13**, 1002183 (2022).
7. Lin, J.-Y., Arthurs, J. & Reilly, S. The effects of amygdala and cortical inactivation on taste neophobia. *Neurobiol. Learn. Mem.* **155**, 322–329 (2018).
8. Wright, G. A. *et al.* Parallel reinforcement pathways for conditioned food aversions in the honeybee. *Current biology : CB* **20**, 2234–2240 (2010).
9. Yao, Z. & Scott, K. Serotonergic neurons translate taste detection into internal nutrient regulation. *Neuron* **110**, 1036-1050.e7 (2022).
10. Yu, S., Luo, F., Xu, Y., Zhang, Y. & Jin, L. H. Drosophila Innate Immunity Involves Multiple Signaling Pathways and Coordinated Communication Between Different Tissues. *Front Immunol* **13**, 905370 (2022).
11. Shim, J. *et al.* Olfactory Control of Blood Progenitor Maintenance. *Cell* **155**, 1141–1153 (2013).
12. Banerjee, U., Girard, J. R., Goins, L. M. & Spratford, C. M. Drosophila as a Genetic Model for Hematopoiesis. *Genetics* **211**, 367–417 (2019).
13. Tokusumi, Y., Tokusumi, T., Stoller-Conrad, J. & Schulz, R. A. Serpent, Suppressor of Hairless and U-shaped are crucial regulators of hedgehog niche expression and prohemocyte maintenance during Drosophila larval hematopoiesis. *Development* **137**, 3561–3568 (2010).
14. Krzemień, J. *et al.* Control of blood cell homeostasis in Drosophila larvae by the posterior signalling centre. *Nature* **446**, 325–328 (2007).
15. Cho, B. *et al.* Single-cell transcriptome maps of myeloid blood cell lineages in Drosophila. *Nat. Commun.* **11**, 4483 (2020).
16. Mandal, L., Martinez-Agosto, J. A., Evans, C. J., Hartenstein, V. & Banerjee, U. A Hedgehog- and Antennapedia-dependent niche maintains Drosophila haematopoietic precursors. *Nature* **446**, 320–324 (2007).
17. Jung, S.-H., Evans, C. J., Uemura, C. & Banerjee, U. The Drosophila lymph gland as a developmental model of hematopoiesis. *Development* **132**, 2521–2533 (2005).
18. Bland, M. L. Regulating metabolism to shape immune function: Lessons from Drosophila. *Semin Cell Dev Biol* **138**, 128–141 (2023).
19. Lu, Y. *et al.* Pattern recognition receptors in Drosophila immune responses. *Dev Comp Immunol* **102**, 103468 (2020).
20. Masuzzo, A., Manière, G., Grosjean, Y., Kurz, L. & Royet, J. Bacteria-derived peptidoglycan triggers a non-canonical NF-κB dependent response in Drosophila gustatory neurons. *J Neurosci* JN-RM-2437-21 (2022) doi:10.1523/jneurosci.2437-21.2022.
21. Montanari, M. *et al.* Larval microbiota primes the Drosophila adult gustatory response. *Nat. Commun.* **15**, 1341 (2024).
22. Dus, M., Min, S., Keene, A. C., Lee, G. Y. & Suh, G. S. B. Taste-independent detection of the caloric content of sugar in Drosophila. *Proceedings of the National Academy of Sciences of the United States of America* **108**, 11644–11649 (2011).
23. Dus, M., Ai, M. & Suh, G. S. B. Taste-independent nutrient selection is mediated by a brain-specific Na+ /solute co-transporter in Drosophila. *Nature neuroscience* **16**, 526–528 (2013).

24. Musso, P.-Y., Tchenio, P. & Preat, T. Delayed dopamine signaling of energy level builds appetitive long-term memory in Drosophila. *Cell reports* **10**, 1023–1031 (2015).
25. Boll, W. & Noll, M. The Drosophila Pox neuro gene: control of male courtship behavior and fertility as revealed by a complete dissection of all enhancers. *Development* **129**, 5667–5681 (2002).
26. LeDue, E. E., Chen, Y.-C., Jung, A. Y., Dahanukar, A. & Gordon, M. D. Pharyngeal sense organs drive robust sugar consumption in Drosophila. *Nature communications* **6**, 6667 (2015).
27. Dweck, H. K. M. & Carlson, J. R. Molecular Logic and Evolution of Bitter Taste in Drosophila. *Curr. Biol.* **30**, 17-30.e3 (2020).
28. Jaeger, A. H. *et al.* A complex peripheral code for salt taste in Drosophila. *eLife* **7**, 44 (2018).
29. McDowell, S. A. T., Stanley, M. & Gordon, M. D. A molecular mechanism for high salt taste in Drosophila. *Curr Biol* **32**, 3070-3081.e5 (2022).
30. Guillemin, J. *et al.* Taste cells expressing Ionotropic Receptor 94e reciprocally impact feeding and egg laying in Drosophila. *bioRxiv* 2024.01.23.576843 (2024) doi:10.1101/2024.01.23.576843.
31. Marella, S. *et al.* Imaging taste responses in the fly brain reveals a functional map of taste category and behavior. *Neuron* **49**, 285–295 (2006).
32. Wang, Z., Singhvi, A., Kong, P. & Scott, K. Taste representations in the Drosophila brain. *Cell* **117**, 981–991 (2004).
33. Apostolopoulou, A. A., Rist, A. & Thum, A. S. Taste processing in Drosophila larvae. *Frontiers in integrative neuroscience* **9**, 50 (2015).
34. Klapoetke, N. C. *et al.* Independent optical excitation of distinct neural populations. *Nature methods* **11**, 338–346 (2014).
35. Soldano, A. *et al.* Gustatory-mediated avoidance of bacterial lipopolysaccharides via TRPA1 activation in Drosophila. *Elife* **5**, e13133 (2016).
36. Chen, Y.-C. D. & Dahanukar, A. Recent advances in the genetic basis of taste detection in Drosophila. *Cell. Mol. Life Sci.* **77**, 1087–1101 (2020).
37. Leung, N. Y. *et al.* Functions of Opsins in Drosophila Taste. *Curr Biol* **30**, 1367-1379.e6 (2020).
38. Gottar, M. *et al.* The Drosophila immune response against Gram-negative bacteria is mediated by a peptidoglycan recognition protein. *Nature* **416**, 640–644 (2002).
39. Maillet, F., Bischoff, V., Vignal, C., Hoffmann, J. & Royet, J. The Drosophila Peptidoglycan Recognition Protein PGRP-LF Blocks PGRP-LC and IMD/JNK Pathway Activation. *Cell Host Microbe* **3**, 293–303 (2008).
40. Gendrin, M. *et al.* Functional Analysis of PGRP-LA in Drosophila Immunity. *Plos One* **8**, e69742 (2013).
41. Basbous, N. *et al.* The Drosophila peptidoglycan-recognition protein LF interacts with peptidoglycan-recognition protein LC to downregulate the Imd pathway. *EMBO Rep.* **12**, 327–333 (2011).
42. Charroux, B. & Royet, J. Elimination of plasmatocytes by targeted apoptosis reveals their role in multiple aspects of the Drosophila immune response. *Proc National Acad Sci* **106**, 9797–9802 (2009).
43. Xi, R., Zheng, X. & Tizzano, M. Role of Taste Receptors in Innate Immunity and Oral Health. *J. Dent. Res.* **101**, 759–768 (2022).
44. Talay, M. *et al.* Transsynaptic Mapping of Second-Order Taste Neurons in Flies by trans-Tango. *Neuron* **96**, 783-795.e4 (2017).
45. Weber, D., Vogt, K., Miroschnikow, A., Pankratz, M. & Thum, A. S. Four Individually Identified Paired Dopamine Neurons Signal Taste Punishment in Larval Drosophila. (2023) doi:10.7554/elife.91387.1.
46. Engert, S., Sterne, G. R., Bock, D. D. & Scott, K. Drosophila gustatory projections are segregated by taste modality and connectivity. *Elife* **11**, e78110 (2022).
47. Kim, H., Kirkhart, C. & Scott, K. Long-range projection neurons in the taste circuit of Drosophila. *eLife* **6**, 13819 (2017).
48. Goyal, M., Tomar, A., Madhwal, S. & Mukherjee, T. Blood progenitor redox homeostasis through olfaction-derived systemic GABA in hematopoietic growth control in Drosophila. *Development* **149**, dev199550 (2022).
49. Rodrigues, D., Renaud, Y., VijayRaghavan, K., Waltzer, L. & Inamdar, M. S. Differential activation of JAK-STAT signaling reveals functional compartmentalization in Drosophila blood progenitors. *Elife* **10**, e61409 (2021).
50. Shim, J., Mukherjee, T. & Banerjee, U. Direct sensing of systemic and nutritional signals by haematopoietic progenitors in Drosophila. *Nat. Cell Biol.* **14**, 394–400 (2012).
51. Madhwal, S. *et al.* Metabolic control of cellular immune-competency by odors in Drosophila. *eLife* **9**, e60376 (2020).
52. Arntsen, C., Guillemin, J., Audette, K. & Stanley, M. Tastant-receptor interactions: insights from the fruit fly. *Front. Nutr.* **11**, 1394697 (2024).
53. Xiao, S., Baik, L. S., Shang, X. & Carlson, J. R. Meeting a threat of the Anthropocene: Taste avoidance of metal ions by Drosophila. *Proc. Natl. Acad. Sci.* **119**, e2204238119 (2022).
54. Luo, R. *et al.* Molecular basis and homeostatic regulation of Zinc taste. *Protein Cell* **13**, 462–469 (2021).
55. Li, X. *et al.* Taste coding of heavy metal ion-induced avoidance in Drosophila. *iScience* **26**, 106607 (2023).
56. Devineni, A. V., Sun, B., Zhukovskaya, A. & Axel, R. Acetic acid activates distinct taste pathways in Drosophila to elicit opposing, state-dependent feeding responses. *eLife* **8**, e47677 (2019).
57. Rimal, S. *et al.* Mechanism of Acetic Acid Gustatory Repulsion in Drosophila. *Cell Rep.* **26**, 1432-1442.e4 (2019).
58. Aryal, B., Dhakal, S., Shrestha, B. & Lee, Y. Molecular and neuronal mechanisms for amino acid taste perception in the Drosophila labellum. *Curr Biol* **32**, 1376-1386.e4 (2022).
59. Mi, T. *et al.* Alkaline taste sensation through the alkaliphile chloride channel in Drosophila. *Nat. Metab.* **5**, 466–480 (2023).
60. Maier, G. L., Komarov, N., Meyenhofer, F., Kwon, J. Y. & Sprecher, S. G. Taste sensing and sugar detection mechanisms in Drosophila larval primary taste center. *Elife* **10**, e67844 (2021).
61. Apostolopoulou, A. A., Mazija, L., Wüst, A. & Thum, A. S. The neuronal and molecular basis of quinine-dependent bitter taste signaling in Drosophila larvae. *Frontiers in behavioral neuroscience* **8**, 6 (2014).

62. Medzhitov, R. & Janeway, CharleS. J. Innate immune recognition: mechanisms and pathways. *Immunol. Rev.* **173**, 89–97 (2000).
63. Aymeric, J.-L., Givaudan, A. & Duvic, B. Imd pathway is involved in the interaction of Drosophila melanogaster with the entomopathogenic bacteria, Xenorhabdus nematophila and Photorhabdus luminescens. *Mol. Immunol.* **47**, 2342–2348 (2010).
64. Arch, M., Vidal, M., Koiffman, R., Melkie, S. T. & Cardona, P.-J. Drosophila melanogaster as a model to study innate immune memory. *Front Microbiol* **13**, 991678 (2022).
65. Bosch, P. S. *et al.* Adult Drosophila Lack Hematopoiesis but Rely on a Blood Cell Reservoir at the Respiratory Epithelia to Relay Infection Signals to Surrounding Tissues. *Dev. Cell* **51**, 787-803.e5 (2019).
66. Koranteng, F., Cho, B. & Shim, J. Intrinsic and Extrinsic Regulation of Hematopoiesis in Drosophila. *Mol Cells* **45**, 101–108 (2022).
67. Bhatt, P. K. & Neckameyer, W. S. Functional Analysis of the Larval Feeding Circuit in *Drosophila*. *J. Vis. Exp.* e51062 (2013) doi:10.3791/51062.
68. Zhan, Y. P., Liu, L. & Zhu, Y. Taotie neurons regulate appetite in Drosophila. *Nat. Commun.* **7**, 13633 (2016).
69. Honjo, K., Hwang, R. Y. & Tracey, W. D. Optogenetic manipulation of neural circuits and behavior in Drosophila larvae. *Nature protocols* **7**, 1470–1478 (2012).
70. Wat, L. W. *et al.* A role for triglyceride lipase brummer in the regulation of sex differences in Drosophila fat storage and breakdown. *Plos Biol* **18**, e3000595 (2020).

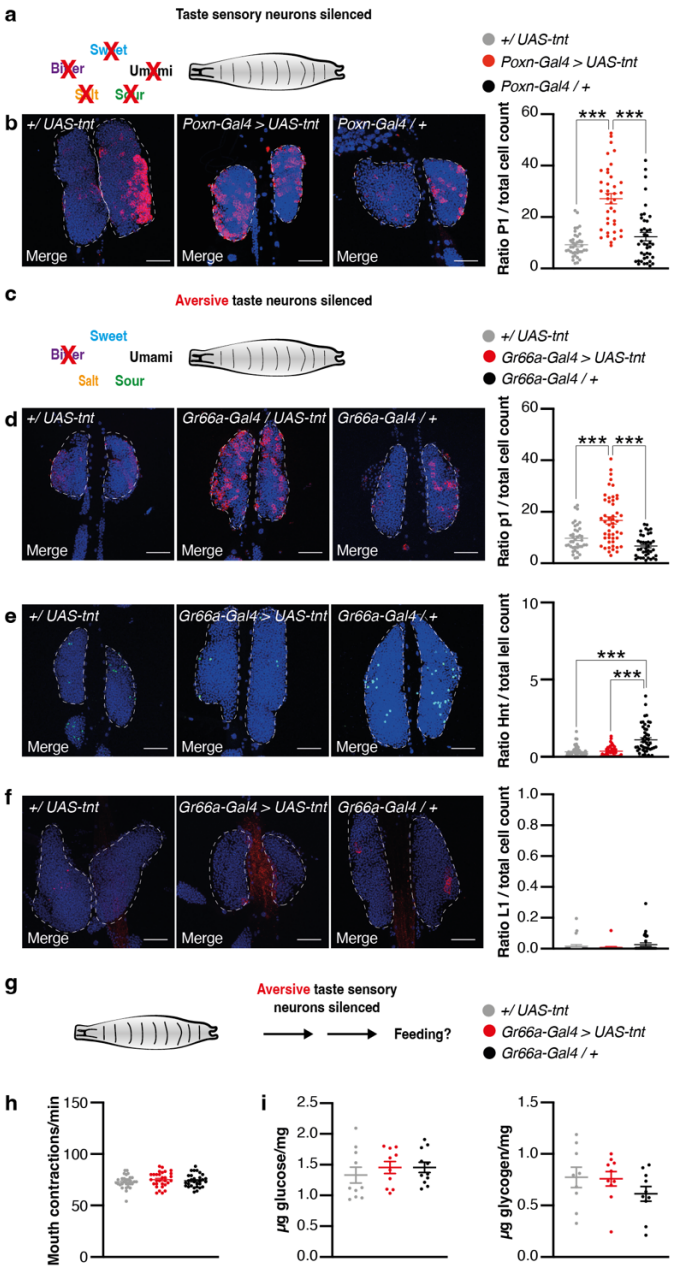

Fig. 1 Silencing bitter taste sensory neurons promotes plasmatocyte differentiation.
a, Schematic showing taste sensory modalities impaired in *Poxn-Gal4>UAS-tnt* larvae. **b**, Staining of lymph gland nuclei (Topro-blue) and differentiated cells (left, P1-red) of *+/UAS-tnt* (n = 37), *Poxn-Gal4>UAS-tnt* (n = 39), *Poxn-Gal4/+* (n = 41) larvae, and quantification of the ratio between the 2 (right). **c**, Schematic showing taste sensory modalities impaired in *Gr66a-Gal4>UAS-tnt* larvae. **d**, Staining of lymph gland nuclei (Topro-blue) and differentiated plasmatocyte cells (left, P1-red) of *+/UAS-tnt* (n = 37), *Gr66a-Gal4>UAS-tnt* (n = 50), *Gr66a-Gal4/+* larvae (n = 39), and quantification of the ratio between the 2 (right). **e**, Staining of lymph gland nuclei (Topro-blue) and differentiated crystal cells (left, Hnt-green) of *+/UAS-tnt* (n = 51), *Gr66a-Gal4>UAS-tnt* (n = 42), *Gr66a-Gal4/+* larvae (n = 49), and quantification of the ratio between the 2 (right). **f**, Staining of lymph gland nuclei (Topro-blue) and differentiated lamellocyte cells (left, L1-red) of *+/UAS-tnt* (n = 26), *Gr66a-Gal4>UAS-tnt* (n = 16), *Gr66a-Gal4/+* larvae (n = 31), and quantification of the ratio between the 2 (right). **g**, Does silencing aversive taste sensing neurons impact feeding? **h**, Number of mouth contraction per minutes on standard food of *+/UAS-tnt* (n = 30), *Gr66a-Gal4>UAS-tnt* (n = 30), *Gr66a-Gal4/+* larvae (n = 30). **i**, Glucose (left) and glycogen (right) from *+/UAS-tnt* (n = 30), *Gr66a-Gal4>UAS-tnt* (n = 30), *Gr66a-Gal4/+* larvae (n = 30) raised on standard food. Scale bars are 50 µm. Values represent mean ± SEM. Statistical tests: one-way ANOVA and Tukey post hoc; $^{**}P < 0.01$; $^{***}P < 0.001$. See also Extended Data Fig. 1.

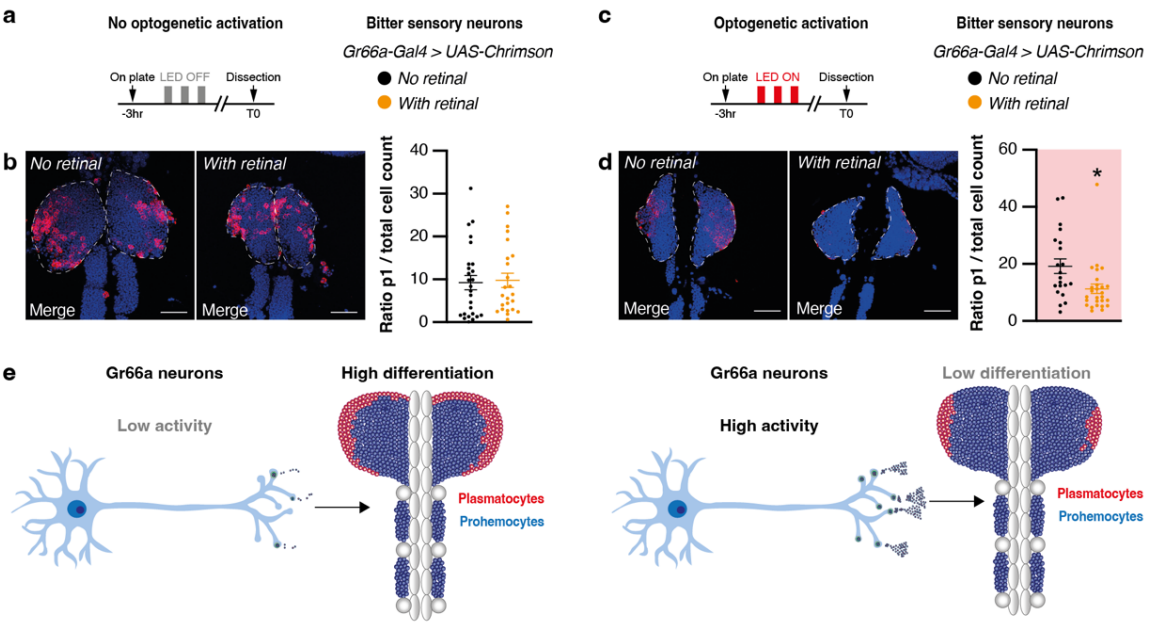

Fig. 2. Optogenetic activation of bitter taste sensory neurons inhibits hematopoiesis.
a, Schematic showing optogenetic protocol, the OFF light does not activate Gr66a neurons. **b**, Staining of lymph gland nuclei (Topro-blue) and differentiated cells (left, P1-red) and quantification of the ratio between the 2 (right) in non-retinal fed larvae (n = 26), and retinal fed larvae (n = 24). **c**, Schematic showing optogenetic protocol, the ON light activates Gr66a neurons in retinal flies. **d**, Staining of lymph gland nuclei (Topro-blue) and differentiated cells (left, P1-red) and quantification of the ratio between the 2 (right)in non-retinal fed larvae (n = 18), and retinal fed larvae (n = 18). **e**, When Gr66a neurons' activity is low, hematopoiesis is high (left). When Gr66a neurons' activity is high, hematopoiesis is low (right). Scale bars are 50 µm. Values represent mean ± SEM. Statistical tests: one-way ANOVA and Tukey post hoc; *$P < 0.05$. See also Extended Data Fig. 2.

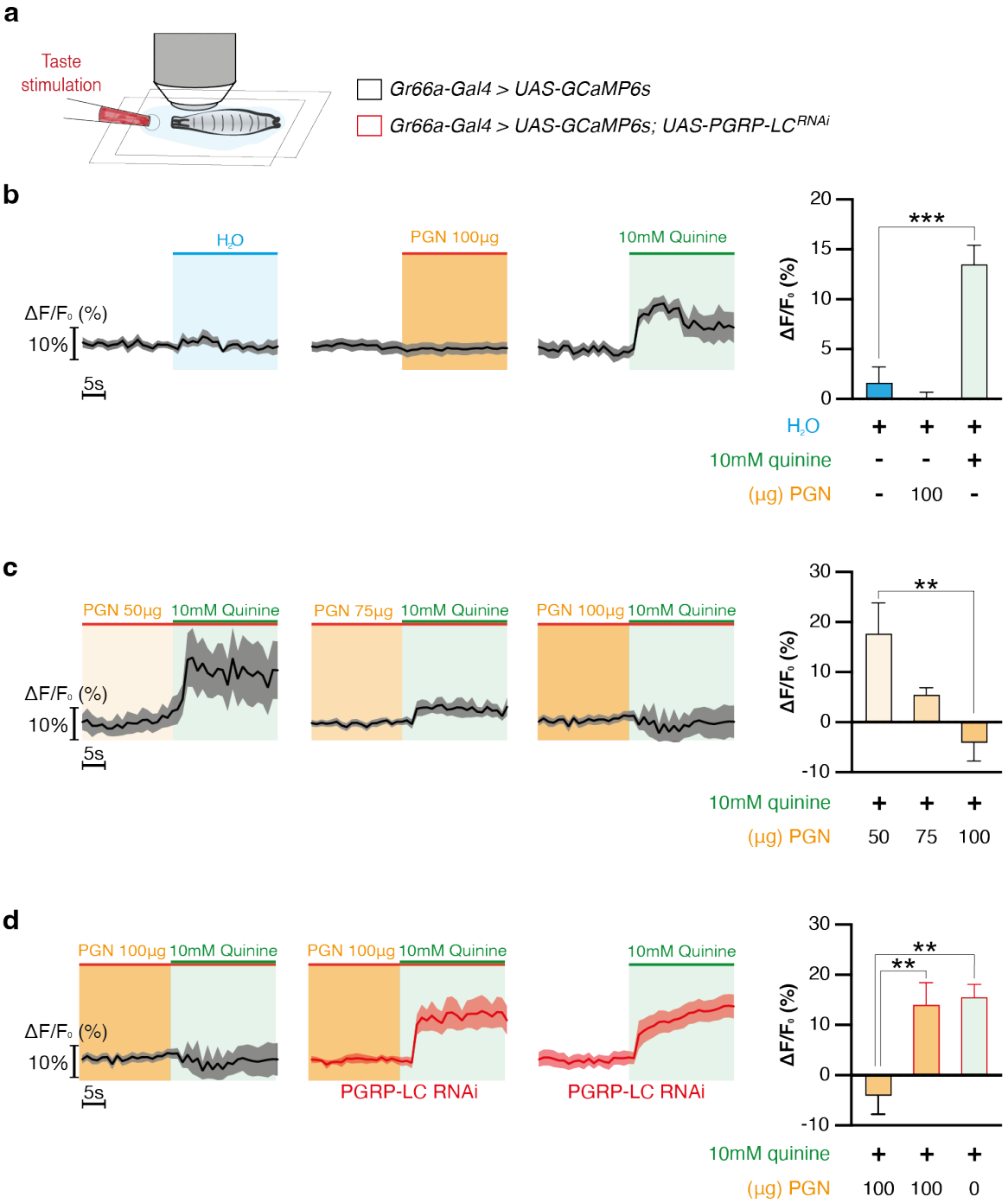

Fig. 3. Peptidoglycan sensing inhibits Gr66a taste sensory neurons.
a, *In vivo* larvae receive taste stimulation directly under the microscope and Gr66a neural activity is monitored in control background or in PGRP-LC knocked down background. **b**, Averaged curves of Gr66a neural activity in response to H_2O ($n = 8$), peptidoglycan ($n = 7$), or quinine ($n = 8$) (left); and quantification of the responses (right). **c**, Averaged curves of Gr66a neural activity in response to 10mM quinine preceded by peptidoglycan solutions at 50 µg/mL ($n = 8$), 75 µg/mL ($n = 8$), or 100 µg/mL (n = 8) (left); and quantification of the responses (right). **d**, Averaged curves of Gr66a neural activity in response to 10mM quinine preceded by peptidoglycan solutions at 100 µg/mL in control larvae ($n = 8$), in larvae with PGRP-LC knocked down and in response to quinine alone (left); and quantification of the responses (right). Values represent mean ± SEM. Statistical tests: Kruskal-Wallis and Dunn's post hoc; $^{**}P < 0.01$; $^{***}P < 0.001$. See also Extended Data Fig. 4.

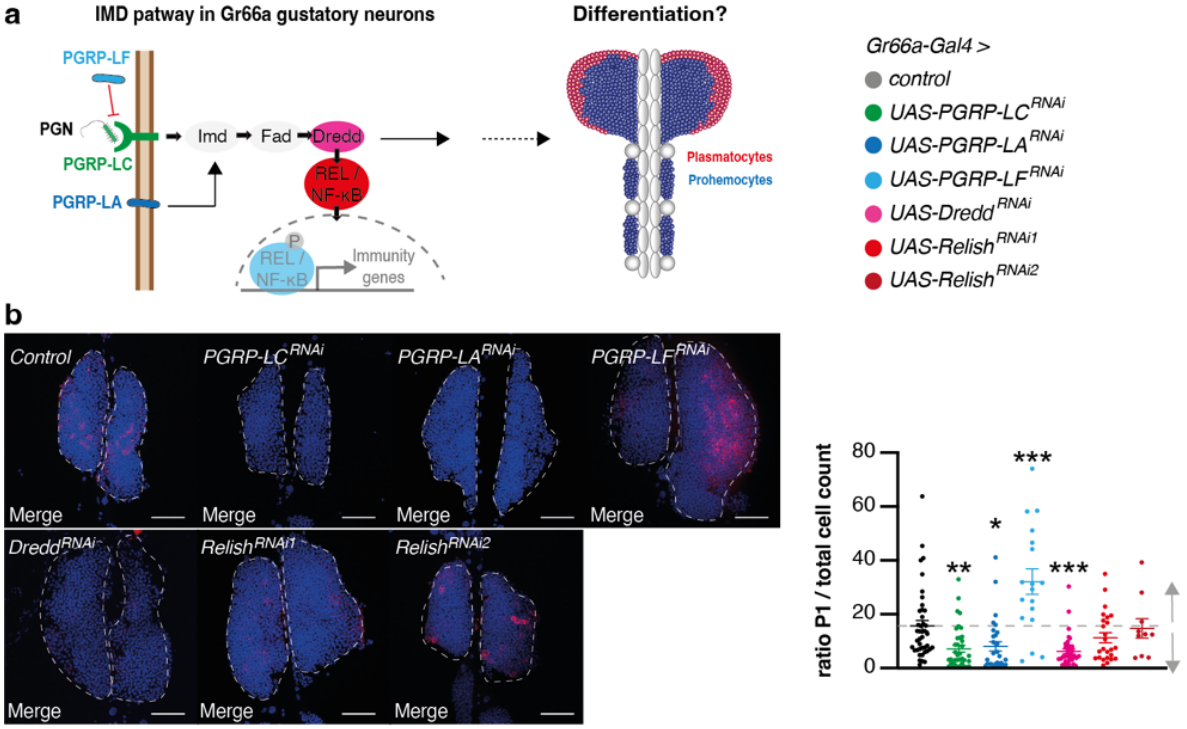

Fig. 4. Knocking down PGRPs and IMD pathway in Gr66a taste sensory neurons inhibits hematopoiesis. **a**, Schematic showing how peptidoglycan detection by the IMD pathway in Gr66a taste sensory neurons could regulate hematopoiesis. **b**, Staining of lymph gland nuclei (Topro-blue) and differentiated cells (left, P1-red) of *Gr66a-Gal4 > IMD* ^{RNAi} larvae (Controls, $n = 42$; PGRP-LC, $n = 38$; PGRP-LA, $n = 30$; PGRP-LF, $n = 18$; Dredd, $n = 39$; Relish, $n = 25$, and 10), and quantification of the ratio between the 2 (right). Scale bars are 50 µm. Values represent mean ± SEM. Statistical tests: one-way ANOVA and Tukey post hoc; $^{*}P < 0.05$; $^{**}P < 0.01$; $^{***}P < 0.001$. See also Extended Data Fig. 5.

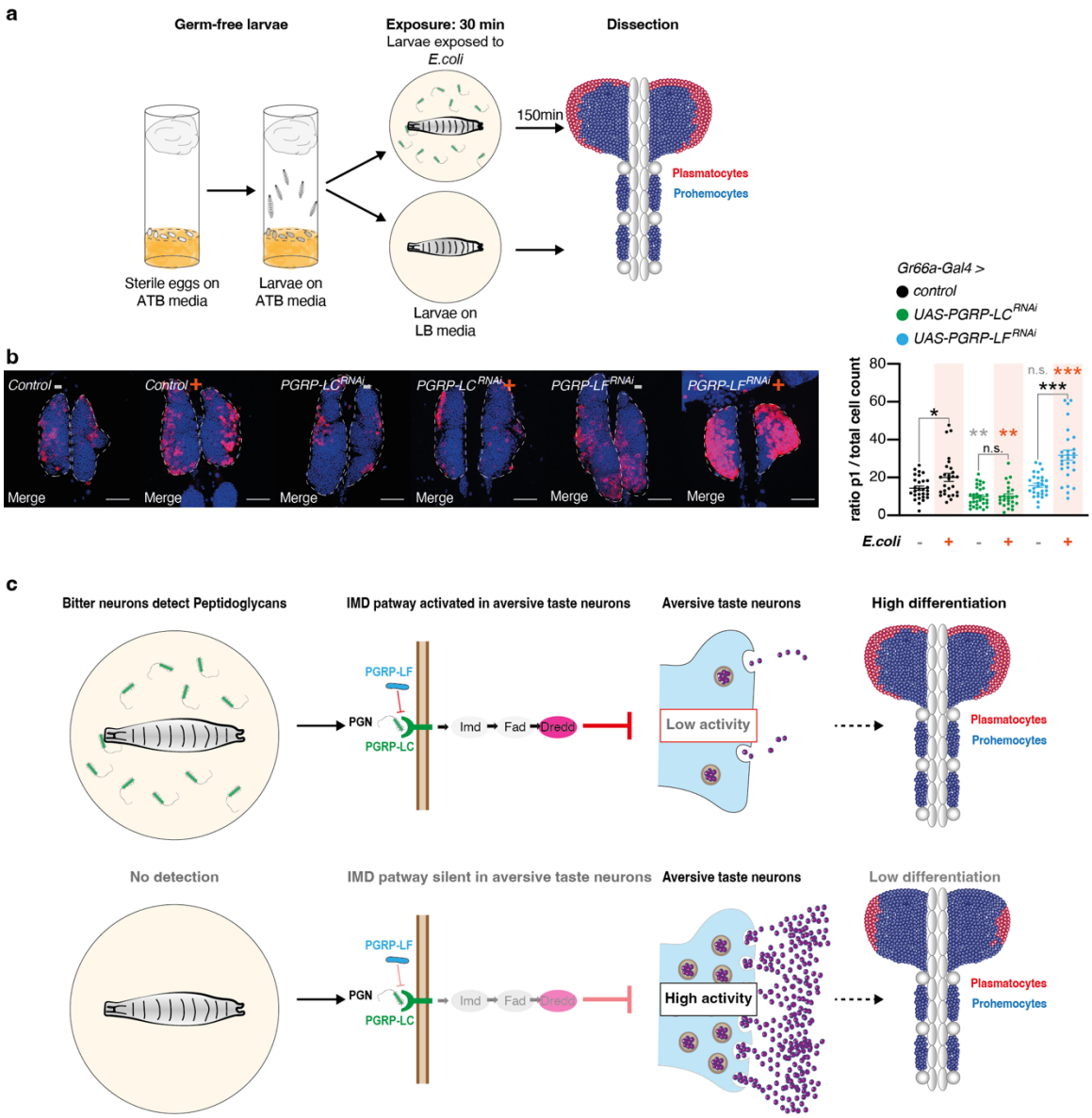

Fig. 5. PGRP-LC in Gr66a gustatory neurons mediates increased hematopoiesis after tasting bacteria. **a**, Schematic representation of the protocol for the exposure of germ-free larvae with *E. coli*. After oviposition the embryos grow under sterile conditions in vials containing ATB media. Then larvae are transferred to LB plates containing either *E. coli* or nothing for 30 minutes and placed back to LB media for 150 minutes before dissection. **b**, Staining of lymph gland nuclei (Topro-blue) and differentiated cells (left, P1-red) of *Gr66a-Gal4 > IMD* ^{RNAi} flies without exposition to *E. coli* (Controls, $n = 28$; PGRP-LC, $n = 32$; PGRP-LF, $n = 28$) and with exposition to *E. coli* (Controls, $n = 27$; PGRP-LC, $n = 24$; PGRP-LF, $n = 28$), and quantification of the ratio between the 2 (right). **c**, In the presence of gram-negative bacteria, larvae detect peptidoglycans through the PGRP-LC/IMD signaling pathway from Gr66a gustatory neurons, which inhibits their activity, thus leading to an increased hematopoiesis. In the absence of Gram- bacteria, the PGRP-LC/IMD signaling pathway from Gr66a gustatory neurons is not activated, which does a release of their inhibition, thus leading to a decreased hematopoiesis. Scale bars are 50 µm. Values represent mean ± SEM. Statistical tests: one-way ANOVA, Tukey post hoc, and unpaired *t*-test for comparison of the same genotype between exposed and non-exposed group; $*P < 0.05$; $**P < 0.01$; $***P < 0.001$. See also Extended Data Fig. 6.

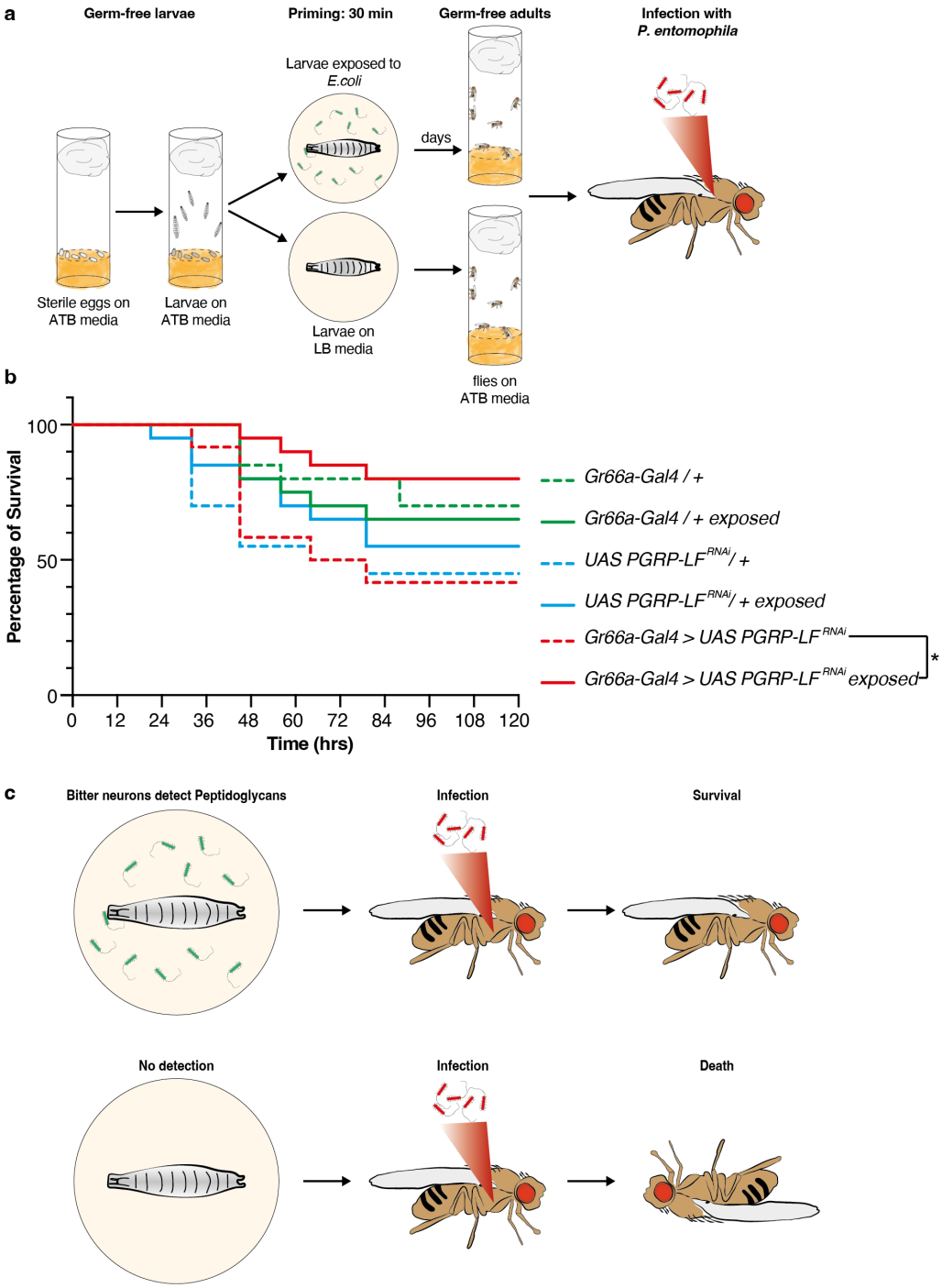

Fig. 6. Overactivation of IMD pathway in Gr66a gustatory neurons primes the cellular immune pathway. **a**, Schematic representation of the protocol for the exposition of germ-free larvae with *E. coli* followed by infection with *P. entomophila* in the adults. After oviposition the embryos grow under sterile conditions into a vial containing ATB media. Then larvae are transferred to LB plates containing either *E. coli* or nothing for 30 minutes and placed back to LB media for 150 minutes. Then the larvae are placed on ATB media until adulthood. Adult flies are then infected by *P.entomophila* and their survival is monitored. **b**, Survival curves following infection with *P.entomophila* of flies previously exposed to *E.coli* (solid lines, *Gr66a-Gal4* > +, n = 20 ; + / *UAS-PGRP-LF*^{RNAi}, n = 20; *Gr66a-Gal4* > *UAS-PGRP-LF*^{RNAi}, n = 19) or to nothing (dashed lines, *Gr66a-Gal4* > + , n = 20 ; + / *UAS-PGRP-LF*^{RNAi}, n = 20; *Gr66a-Gal4* > *UAS-PGRP-LF*^{RNAi}, n = 12). **c**, In the presence of gram-negative bacteria, the activation of the IMD signaling pathway from Gr66a gustatory neurons, promotes higher resistance to infection in adult flies. Values represent mean. Statistical tests: one-sided log-rank test; $^{**}P < 0.01$. See also Extended Data Fig. 7.

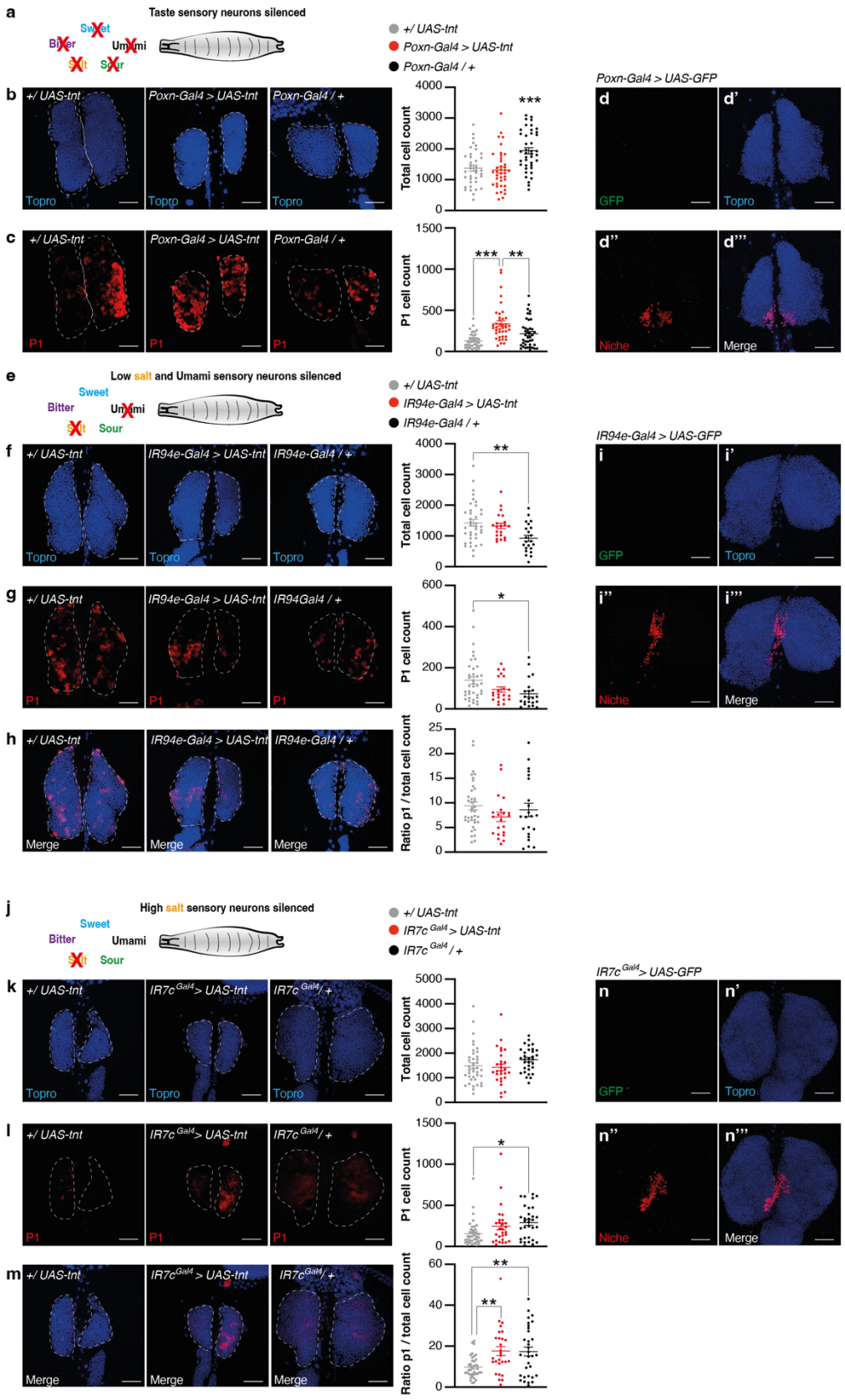
a
Taste sensory neurons silenced
Sweet
Bitter
Umami
Salt
Sour
b
+/ UAS-tnt
Poxn-Gal4 > UAS-tnt
Poxn-Gal4 / +
Topro
c
P1
Total cell count
P1 cell count
***
**
Poxn-Gal4 > UAS-GFP
d
d'
d''
d'''
GFP
Niche
Merge
e
Low salt and Umami sensory neurons silenced
IR94e-Gal4 > UAS-tnt
IR94e-Gal4 / +
f
g
IR94Gal4 / +
h
Ratio p1 / total cell count
*
IR94e-Gal4 > UAS-GFP
i
i'
i''
i'''
j
High salt sensory neurons silenced
IR7c Gal4 > UAS-tnt
IR7c Gal4 / +
k
l
m
IR7c Gal4 > UAS-GFP
n
n'
n''
n'''

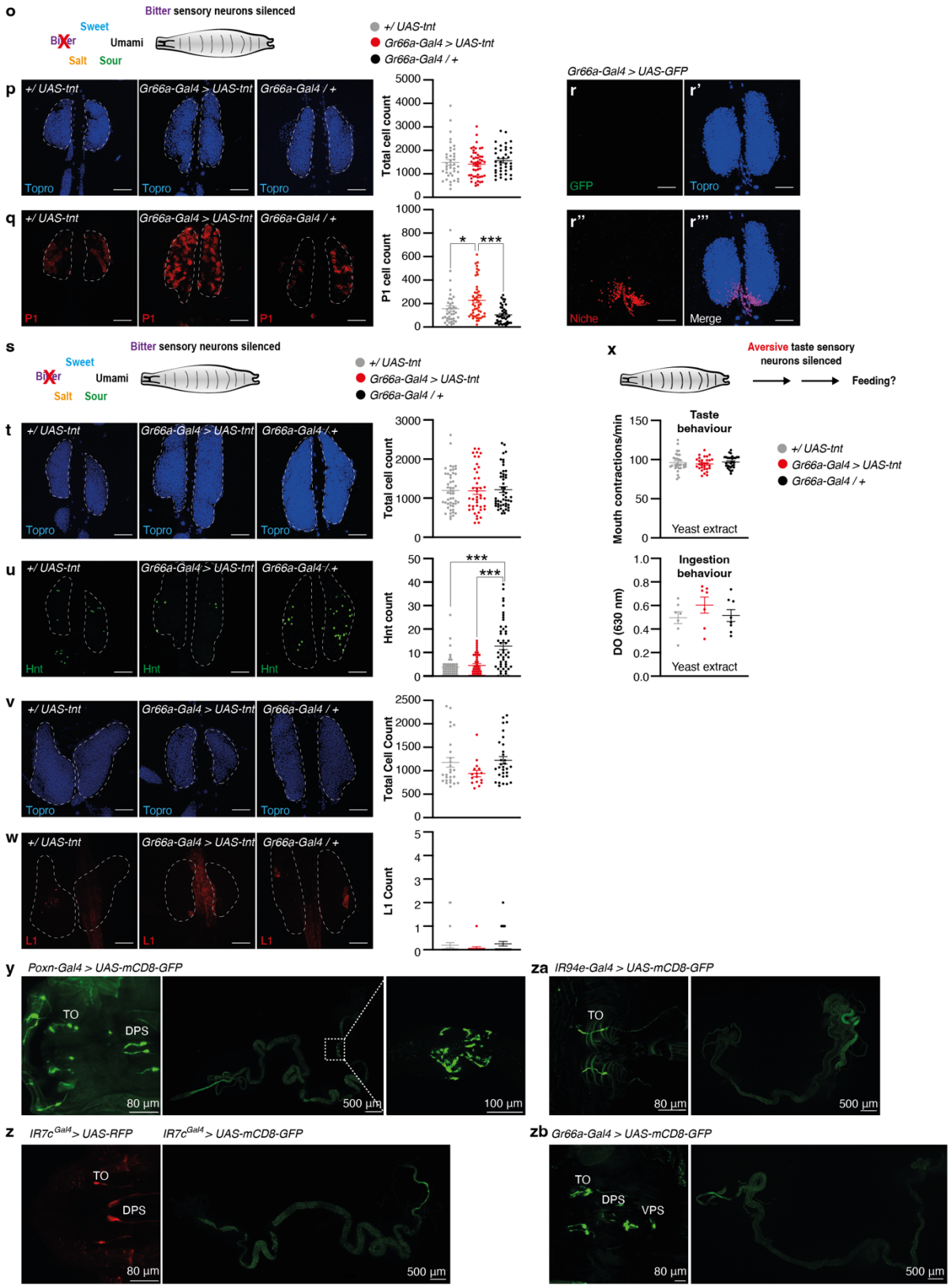

Extended Data Fig. 1. Silencing bitter taste sensory neurons promotes hematopoiesis, related to Fig. 1. **a**, Schematic showing taste sensory modalities impaired in *Poxn-Gal4>UAS-tnt* larvae. **b**, Staining of lymph gland nuclei (left, Topro-blue) of *+/UAS-tnt* ($n = 37$), *Poxn-Gal4>UAS-tnt* ($n = 39$), *Poxn-Gal4/+* ($n = 41$) larvae, and their quantification (right). **c**, Staining of lymph gland differentiated cells (left, P1-red) of *+/UAS-tnt*, *Poxn-Gal4>UAS-tnt*, *Poxn-Gal4/+* larvae, and their quantification (right). **d**, GFP staining of *Poxn-Gal4 >*

UAS-GFP in the lymph gland (GFP-green), **d'**, of the nuclei (Topro-blue), **d''**, of niche cells (Antp-red). **d'''**, Merge of all stainings. **e**, Schematic showing taste sensory modalities impaired in *Ir94e-Gal4>UAS-tnt* larvae. **f**, Staining of lymph gland nuclei (left, Topro-blue) of *+/UAS-tnt* (*n* =37), *Ir94e-Gal4>UAS-tnt* (*n* = 21), *Ir94e-Gal4/+* (*n* = 24) larvae, and their quantification (right). **g**, Staining of lymph gland differentiated cells (left, P1-red) of *+/UAS-tnt, Ir94e-Gal4>UAS-tnt, Ir94e-Gal4 /+* flies, and their quantification (right). **h**, Staining of lymph gland nuclei (Topro-blue) and differentiated cells (left, P1-red) of *+/UAS-tnt* (*n* =37), *Ir94e-Gal4>UAS-tnt* (*n* = 21), *Ir94e-Gal4/+* (*n* = 24) larvae, and quantification of the ratio between the 2 (right). **i**, GFP staining of *Ir94e-Gal4 > UAS-GFP* in the lymph gland (GFP-green), **i'**, of the nuclei (Topro-blue), **i''**, of niche cells (Antp-red). **i'''**, Merge of all stainings. **j**, Schematic showing taste sensory modalities impaired in $Ir7c^{Gal4}$*>UAS-tnt* larvae. **k**, Staining of lymph gland nuclei (left, Topro-blue) of *+/UAS-tnt* (*n* = 39), $Ir7c^{Gal4}$*>UAS-tnt* (*n* = 28), $Ir7c^{Gal4}$*/+* (*n* = 32) larvae, and their quantification (right). **l**, Staining of lymph gland differentiated cells (left, P1-red) of *+/UAS-tnt,* $Ir7c^{Gal4}$*>UAS-tnt,* $Ir7c^{Gal4}$*/+* larvae, and their quantification (right). **m**, Staining of lymph gland nuclei (Topro-blue) and differentiated cells (left, P1-red) of *+/UAS-tnt* (*n* = 39), $Ir7c^{Gal4}$*>UAS-tnt* (*n* = 28), $Ir7c^{Gal4}$*/+* (*n* = 32) larvae, and quantification of the ratio between the 2 (right). **n**, GFP staining of $Ir7c^{Gal4}$*> UAS-GFP* in the lymph gland (GFP-green), **n'**, of the nuclei (Topro-blue), **n''**, of niche cells (Antp-red). **n'''**, Merge of all stainings. **o**, Schematic showing taste sensory modalities impaired in *Gr66a-Gal4>UAS-tnt* larvae. **p**, Staining of lymph gland nuclei (left, Topro-blue) of *+/UAS-tnt* (*n* = 37), *Gr66a-Gal4>UAS-tnt* (*n* = 50), *Gr66a-Gal4/+* flies (*n* = 39), and their quantification (right). **q**, Staining of lymph gland differentiated cells (left, P1-red) of *+/UAS-tnt, Gr66a-Gal4>UAS-tnt, Gr66a-Gal4 /+* larvae, and their quantification (right). **r**, GFP staining of *Gr66a-Gal4 > UAS-GFP* in the lymph gland (GFP-green), **p'**, of the nuclei (Topro-blue), **r''**, of niche cells (Antp-red). **r'''**, Merge of all stainings. **s**, Schematic showing taste sensory modalities impaired in *Gr66a-Gal4>UAS-tnt* larvae. **t**, Staining of lymph gland nuclei (left, Topro-blue) of *+/UAS-tnt* (*n* = 42), *Gr66a-Gal4 > UAS-tnt* (*n* = 34), *Gr66a-Gal4/+* (*n* = 36) larvae, and their quantification (right). **u**, Staining of lymph gland differentiated crystal cells (left, Hnt-green) of *+/UAS-tnt* (*n* = 42), *Gr66a-Gal4 > UAS-tnt* (*n* = 34), *Gr66a-Gal4/+* (*n* = 36) larvae, and their quantification (right). **v**, Staining of lymph gland nuclei (left, Topro-blue) of *+/UAS-tnt* (*n* = 26), *Gr66a-Gal4 > UAS-tnt* (*n* = 16), *Gr66a-Gal4/+* (*n* = 31) larvae, and their quantification (right). **w**, Staining of lymph gland differentiated lamellocytes cells (left, L1-red) of *+/UAS-tnt* (*n* = 26), *Gr66a-Gal4 > UAS-tnt* (*n* = 16), *Gr66a-Gal4/+* (*n* = 31) larvae, and their quantification (right). **x**, Does silencing aversive taste sensing neurons impact feeding? **h**, Number of mouth contraction (top) per minutes on 2% yeast extract of *+/UAS-tnt* (*n* = 30), *Gr66a-Gal4>UAS-tnt* (*n* = 30), *Gr66a-Gal4/+* larvae (*n* = 30); (bottom) food intake on 2% yeast extract of *+/UAS-tnt* (*n* = 7), *Gr66a-Gal4>UAS-tnt* (*n* = 8), *Gr66a-Gal4/+* larvae (*n* = 7). **y**, Staining of Poxn-Gal4>UAS-GFP larvae mouthpart (left) and guts (right). **z**, Staining of Ir94e-Gal4>UAS-GFP larvae mouthpart (left) and guts (right). **za**, Staining of $Ir7c^{Gal4}$>UAS-GFP larvae mouthpart (left) and guts (right). **zb**, Staining of Gr66a-Gal4>UAS-GFP larvae mouthpart (left) and guts (right). TO: Terminal Organ, DPS: Dorsal pharyngeal Sensilla, VPS: Dorsal pharyngeal Sensilla. For A to P''', scale bars are 50 µm. Values represent mean ± SEM. Statistical tests: one-way ANOVA and Tukey post hoc; $*P < 0.05$; $**P < 0.01$; $***P < 0.001$.

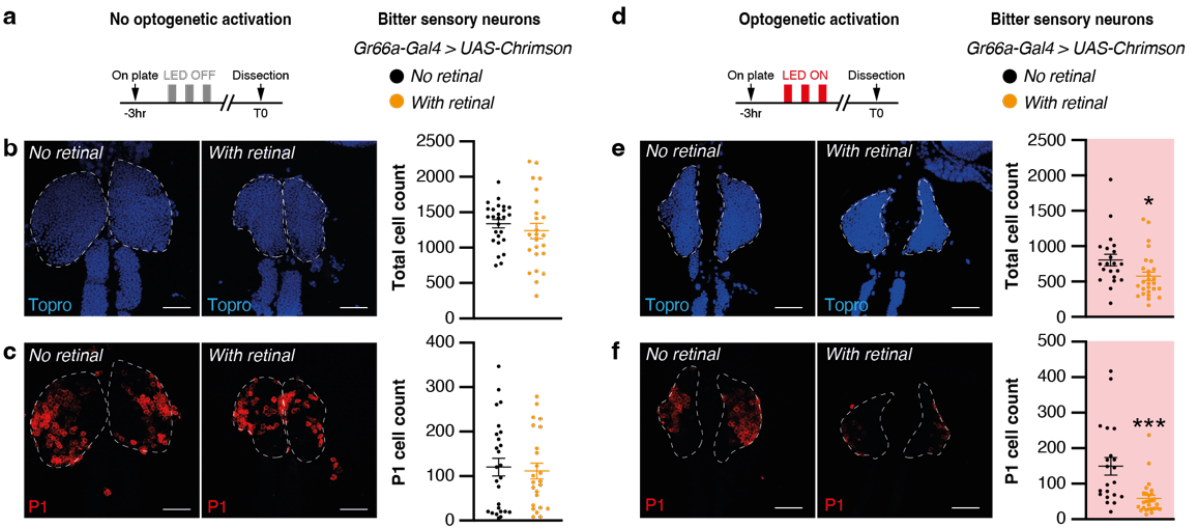

Extended Data Fig. 2. Optogenetic activation of bitter taste sensory neurons inhibits hematopoiesis, related to Fig. 2.

a, Schematic showing optogenetic protocol, the OFF light does not activate Gr66a neurons. **b**, Staining of lymph gland nuclei (left, Topro-blue) and its quantification (right) in non-retinal fed larvae ($n = 26$), and retinal fed larvae ($n = 24$). **c**, Staining of lymph gland differentiated cells (left, P1-red) and its quantification (right). **d**, Schematic showing optogenetic protocol, the ON light activates Gr66a neurons in retinal flies. **e**, Staining of lymph gland nuclei (left, Topro-blue) and its quantification (right) in non-retinal fed larvae ($n = 18$), and retinal fed larvae ($n = 18$). **f**, Staining of lymph gland differentiated cells (left, P1-red) and its quantification (right). Scale bars are 50 µm. Values represent mean ± SEM. Statistical tests: one-way ANOVA and Tukey post hoc; $^{*}P < 0.05$; $^{***}P < 0.001$.

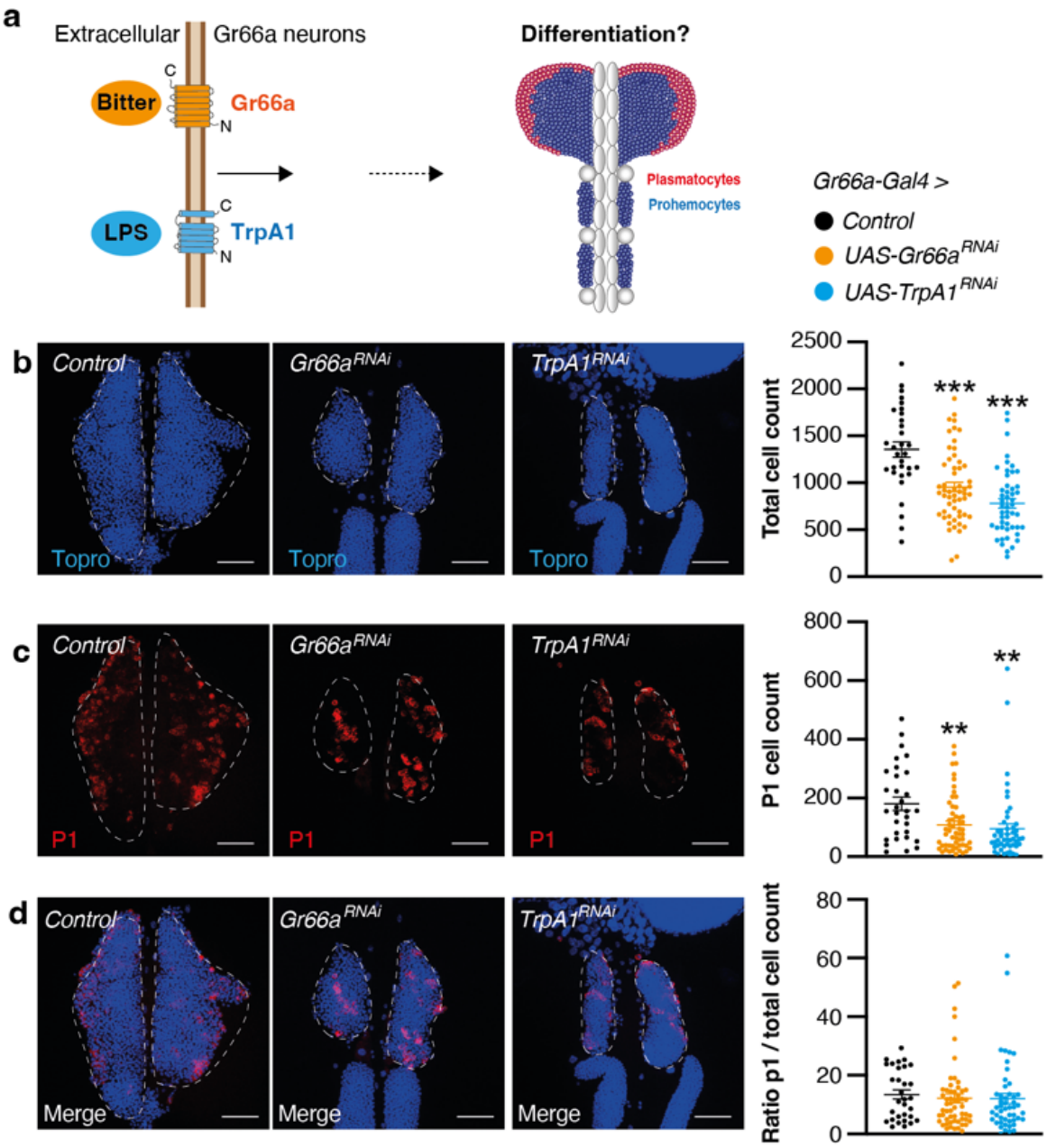

Extended Data Fig. 3. modulating Gr66a and TrPA1 receptors does not modulate hematopoiesis. **a,** Schematic showing TrpA1 and Gr66a receptor expression in Gr66a taste sensory neurons labeled by Gr66a-Gal4. **b,** Staining of lymph gland nuclei (left, Topro-blue) *Gr66a-Gal4 > control* ($n = 31$), *UAS-Gr66a*^{RNAi} ($n = 55$), and *UAS-TrpA1*^{RNAi} ($n = 49$) larvae, and their quantification (right). **c**, Staining of lymph gland differentiated cells (left, P1-red) of *Gr66a-Gal4 > control*, *UAS-Gr66a*^{RNAi}, and *UAS-TrpA1*^{RNAi}, and their quantification (right). **d,** Staining of lymph gland nuclei (Topro-blue) and differentiated cells (left, P1-red) of *Gr66a-Gal4 > control* ($n = 31$), *UAS-Gr66a*^{RNAi} ($n = 55$), and *UAS-TrpA1*^{RNAi} ($n = 49$) flies, and quantification of the ratio between the 2 (right). Scale bars are 50 µm.Values represent mean ± SEM. Statistical tests: one-way ANOVA and Tukey post hoc; $^{*}P < 0.05$; $^{**}P < 0.01$; $^{***}P < 0.001$.

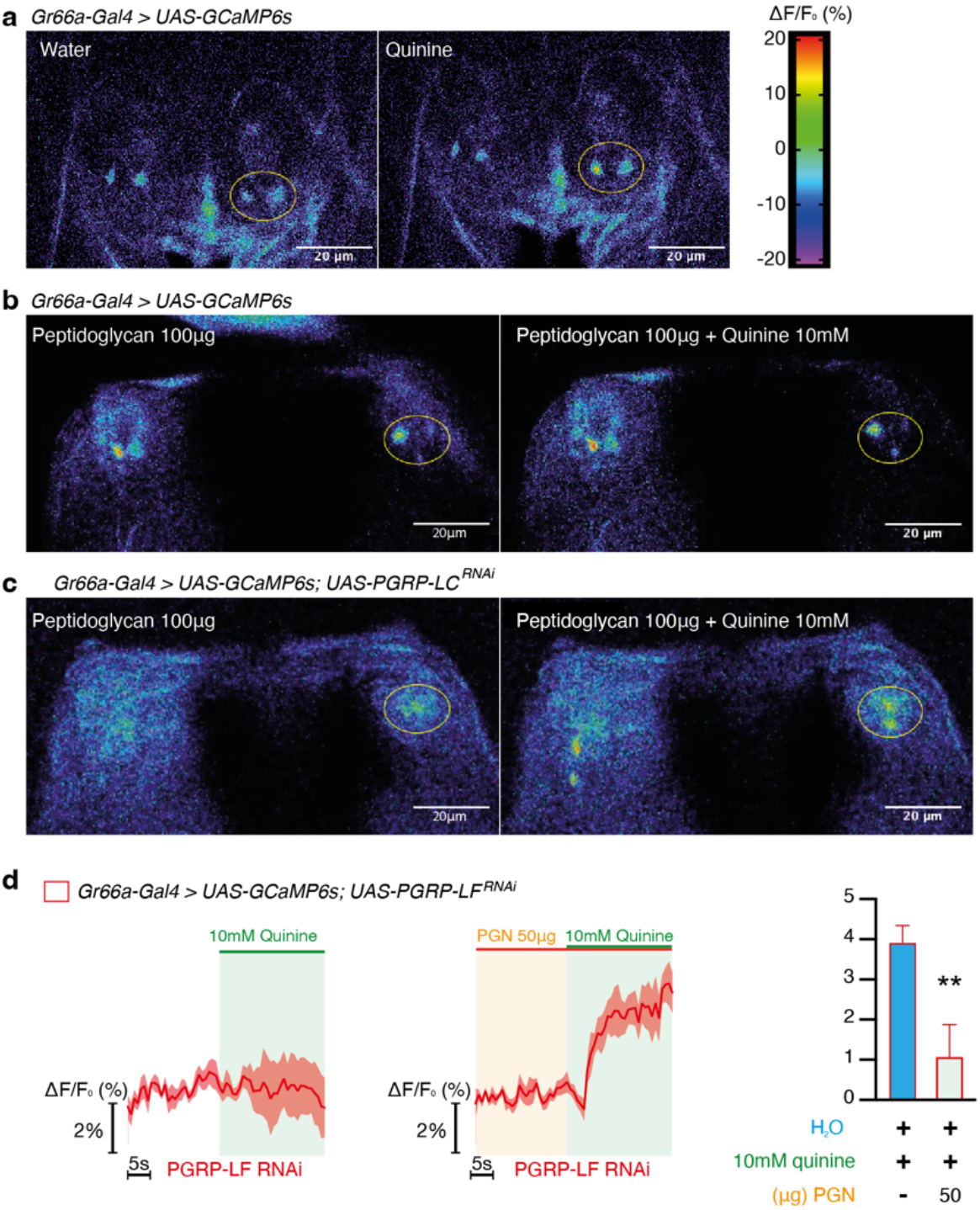

Extended Data Fig. 4. Peptidoglycan sensing inhibits Gr66a taste sensory neurons, related to Fig. 3. **a,** Representative images showing the GCaMP6s intensity before and after addition of either the control Ringer's solution (left panels) or the quinine (right panels) in *Gr66a-Gal4>UAS-GCaMP6s* larvae. **b**, Representative images showing the GCaMP6s intensity before and after addition of either the peptidoglycan solution (left panels) or the quinine+ peptidoglycan (right panels) in *Gr66a-Gal4>UAS-GCaMP6s* larvae. **c**, Representative images showing the GCaMP6s intensity before and after addition of either the peptidoglycan solution (left panels) or the quinine+ peptidoglycan (right panels) in *Gr66a-Gal4>UAS-GCaMP6s; UAS-PGRP-LC* ^{RNAi} larvae. **d,** Averaged curves of Gr66a neural activity in larvae with PGRP-LF knocked down in response to 10mM quinine preceded by H_2O (n = 8) or by peptidoglycan solutions at 50 µg/mL (*n* = 7) (left); and quantification of the responses (right). Values represent mean ± SEM. Statistical tests: Kruskal-Wallis and Dunn's post hoc; $^{**}P < 0.01$.

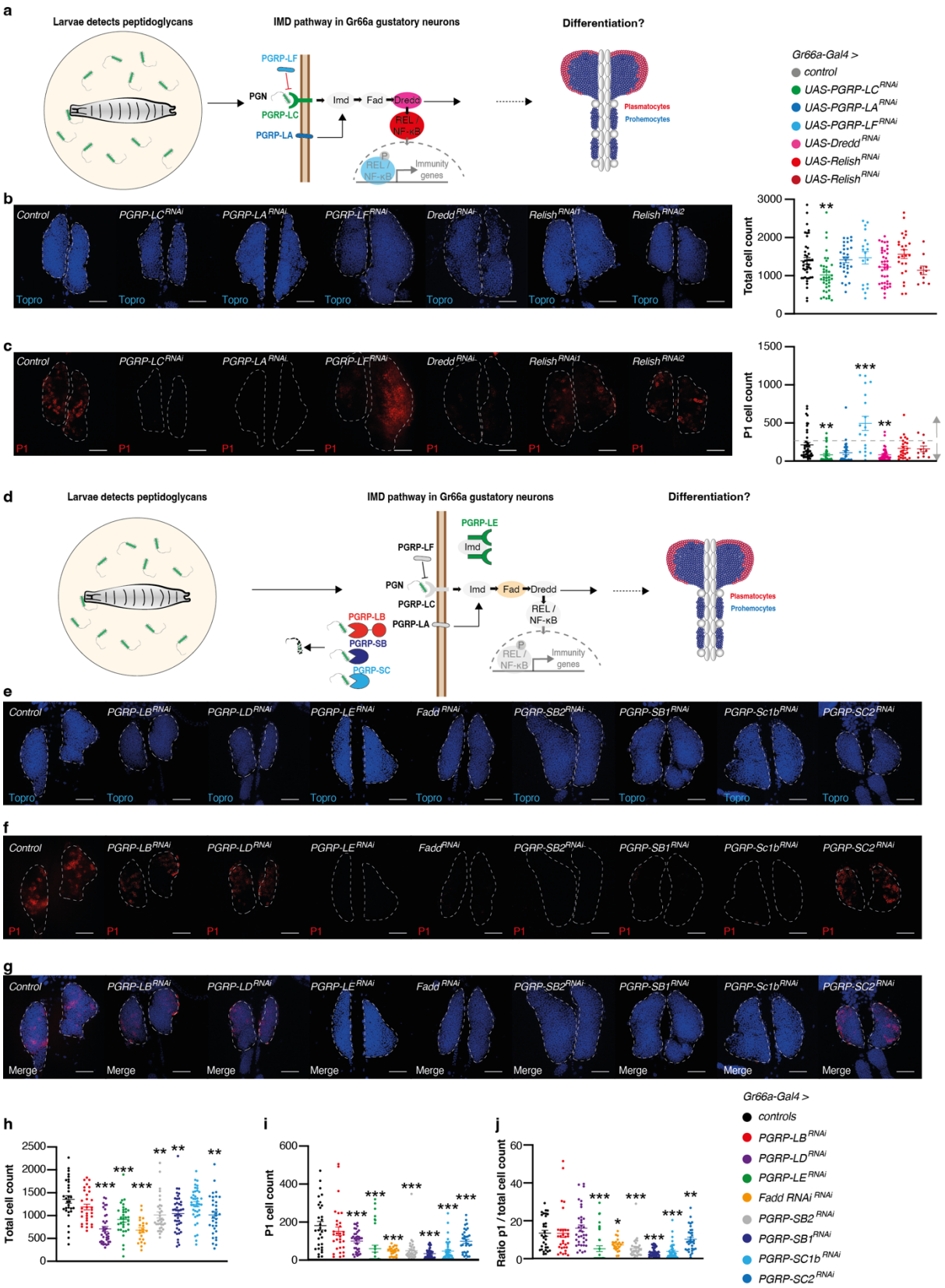
a
Larvae detects peptidoglycans
IMD pathway in Gr66a gustatory neurons
Differentiation?
PGRP-LF
PGN
PGRP-LC
PGRP-LA
Imd
Fad
Dredd
REL / NF-κB
P
Immunity genes
Plasmatocytes
Prohemocytes
Gr66a-Gal4 >
control
UAS-PGRP-LC RNAi
UAS-PGRP-LA RNAi
UAS-PGRP-LF RNAi
UAS-Dredd RNAi
UAS-Relish RNAi
UAS-Relish RNAi
b
Control
PGRP-LC RNAi
PGRP-LA RNAi
PGRP-LF RNAi
Dredd RNAi
Relish RNAi1
Relish RNAi2
Topro
Total cell count
c
P1
P1 cell count
d
PGRP-LE
PGRP-LB
PGRP-SB
PGRP-SC
e
PGRP-LB RNAi
PGRP-LD RNAi
PGRP-LE RNAi
Fadd RNAi
PGRP-SB2 RNAi
PGRP-SB1 RNAi
PGRP-Sc1b RNAi
PGRP-SC2 RNAi
f
g
Merge
h
i
j
Ratio p1 / total cell count
controls

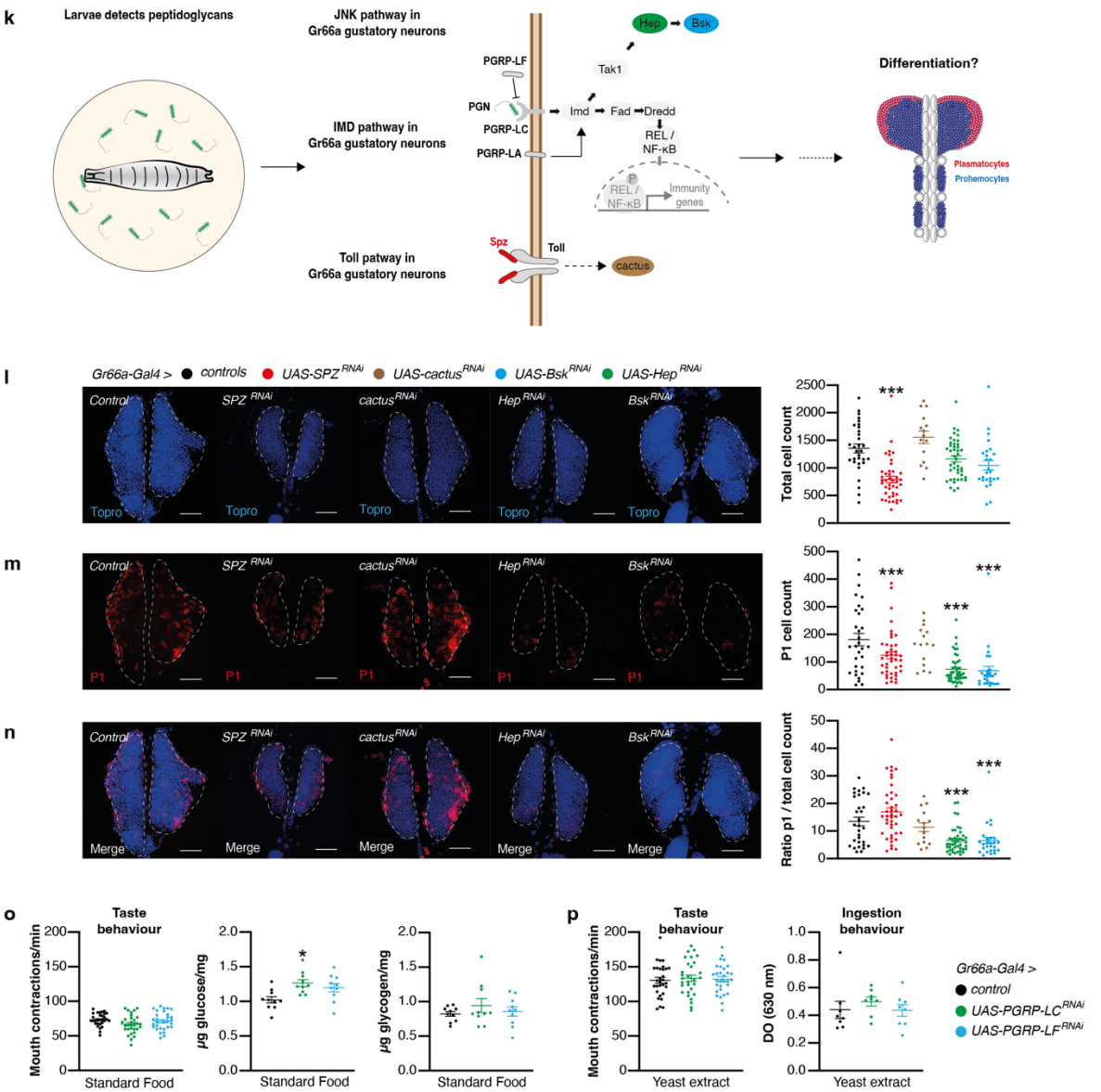

Extended Data Fig. 5. Knocking down PGRPs and IMD pathway in Gr66a taste sensory neurons inhibits hematopoiesis, related to Fig. 5.

a, Schematic showing how peptidoglycan detection by the IMD pathway in Gr66a taste sensory neurons could regulate hematopoiesis. **b**, Staining of lymph gland nuclei (Topro-blue) of *Gr66a-Gal4 > IMD* ^{RNAi} larvae (Controls, n = 42; PGRP-LC, n = 38; PGRP-LA, n = 30; PGRP-LF, n = 18; Dredd, n = 39; Relish, n = 25, and 10), and their quantification (right). **c**, Staining of lymph gland differentiated cells (P1-red) of *Gr66a-Gal4 > IMD* ^{RNAi} larvae, and their quantification (right). **d**, Schematic showing how peptidoglycan detection by the IMD pathway in Gr66a taste sensory neurons could regulate hematopoiesis. **e**, Staining of lymph gland nuclei (Topro-blue) of *Gr66a-Gal4 > IMD* ^{RNAi} larvae. **f**, Staining of lymph gland differentiated cells (P1-red) of *Gr66a-Gal4 > IMD* ^{RNAi} larvae. **g**, Staining of lymph gland nuclei (Topro-blue) and differentiated cells (P1-red) of *Gr66a-Gal4 > IMD* ^{RNAi} larvae.**h**, Quantification of total cell number (Controls, n = 31; PGRP-LB, n = 31; PGRP-LD, n = 36; PGRP-LE, n = 26; Fadd, n = 22; PGRP-SB2, n = 31; PGRP-SB1, n = 42; PGRP-SC1b, n = 41; PGRP-SC2, n = 33). **i**, Quantification of differentiated cells. **j**, Quantification of the ratio of differentiated cells/total number of cells. **k**, Schematic showing how IMD, Toll and JNK pathways in Gr66a taste sensory neurons could regulate hematopoiesis. **l**, Staining of lymph gland nuclei (Topro-blue) of *Gr66a-Gal4 > Toll* ^{RNAi} larvae and *JNK* ^{RNAi} larvae (Controls, n = 31; SPZ, n = 42; cactus, n = 15; Bsk, n = 26; Hep, n = 43), and their quantification (right). **m**, Staining of lymph gland differentiated cells (P1-red) of *Gr66a-Gal4 > Toll* ^{RNAi} larvae and *JNK* ^{RNAi} larvae (Controls, n = 31; SPZ, n = 42; cactus, n = 15; Bsk, n = 26; Hep, n = 43), and their quantification (right). **n**, Staining of lymph gland nuclei (Topro-blue) and differentiated cells (P1-red) of *Gr66a-*

Gal4 > Toll ^{RNAi} larvae and *JNK* ^{RNAi} larvae (Controls, n = 31; SPZ, n = 42; cactus, n = 15; Bsk, n = 26; Hep, n = 43), and their quantification (right). **o,** Number of mouth contraction per minutes on standard food of *Gr66a-Gal4 > IMD* ^{RNAi} larvae (Controls, n = 30; PGRP-LC, n = 30; PGRP-LF, n = 30) (left); Glucose (middle) and glycogen (right) from *Gr66a-Gal4 > IMD* ^{RNAi} larvae (Controls, n =1; PGRP-LC, n = 10; PGRP-LF, n = 10) raised on standard food. **p**, Number of mouth contraction per minutes on 2% yeast extract of *Gr66a-Gal4 > IMD* ^{RNAi} larvae (Controls, n = 30; PGRP-LC, n = 30; PGRP-LF, n = 30) on standard food (left); food intake on 2% yeast extract of *Gr66a-Gal4 > IMD* ^{RNAi} larvae (Controls, n = 8; PGRP-LC, n = 8; PGRP-LF, n = 8). Scale bars are 50 µm. Values represent mean ± SEM. Statistical tests: one-way ANOVA and Tukey post hoc; $^{*}P < 0.05$; $^{**}P < 0.01$; $^{***}P < 0.001$.

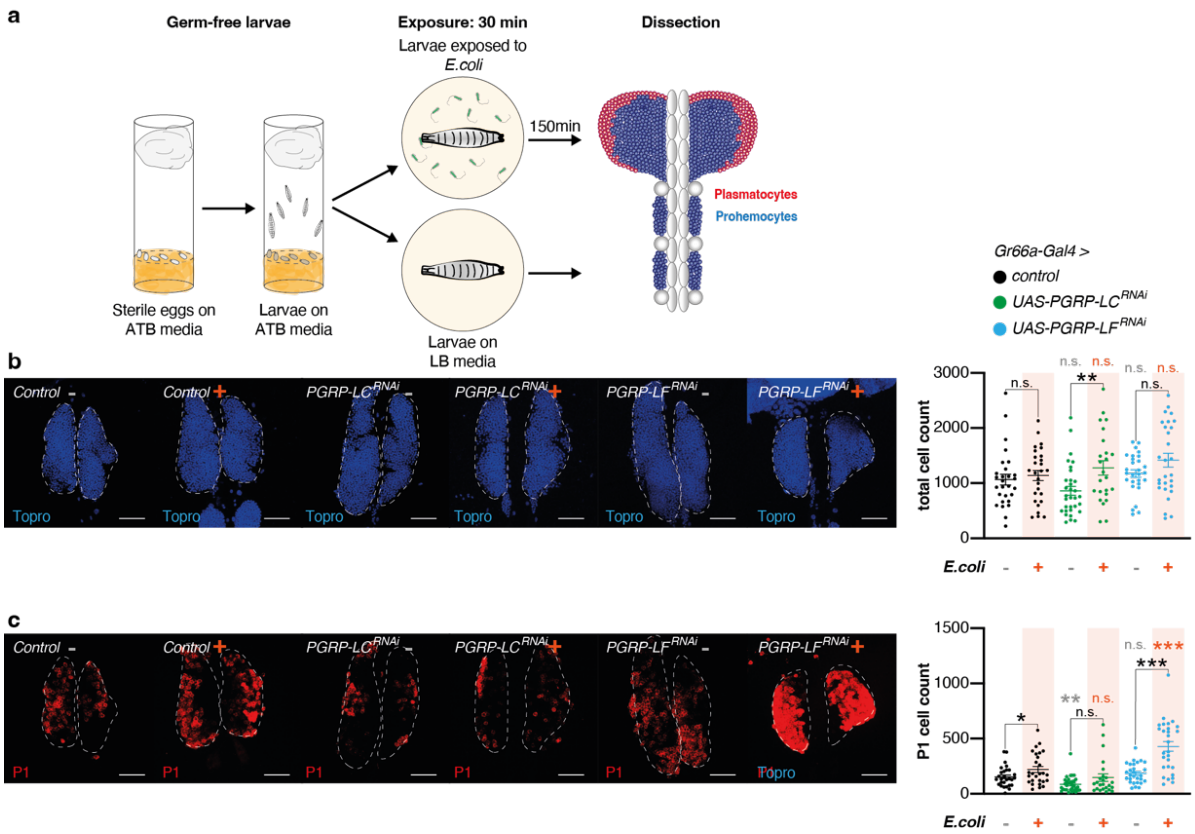

Extended Data Fig. 6. PGRP-LC in Gr66a gustatory neurons mediates increased hematopoiesis after tasting bacteria, related to Fig. 6.

a, Schematic representation of the protocol for the exposition of germ-free larvae with *E. coli*. Embryos grow under sterile conditions into a fresh vial containing ATB media. Then larvae are transferred to LB plates containing either *E. coli* or nothing for 30 minutes and placed back to LB media for 150 minutes before dissection.**b**, Staining of lymph gland nuclei (left, Topro-blue) of *Gr66a-Gal4 > IMD* ^{RNAi} flies without exposition to *E. coli* (Controls, $n = 28$; PGRP-LC, $n = 32$; PGRP-LF, $n = 28$) and with exposition to *E. coli* (Controls, $n = 27$; PGRP-LC, $n = 24$; PGRP-LF, $n = 28$), and quantification (right). **c**, Staining of lymph differentiated cells (left, P1-red) of *Gr66a-Gal4 > IMD* ^{RNAi} flies without exposition to *E. coli* (Controls, $n = 28$; PGRP-LC, $n = 32$; PGRP-LF, $n = 28$) and with exposition to *E. coli* (Controls, $n = 27$; PGRP-LC, $n = 24$; PGRP-LF, $n = 28$), and quantification (right). Scale bars are 50 µm. Values represent mean ± SEM. Statistical tests: one-way ANOVA, Tukey post hoc, and unpaired *t*-test for comparison of the same genotype between exposed and non-exposed group; $*P < 0.05$; $**P < 0.01$; $***P < 0.001$.

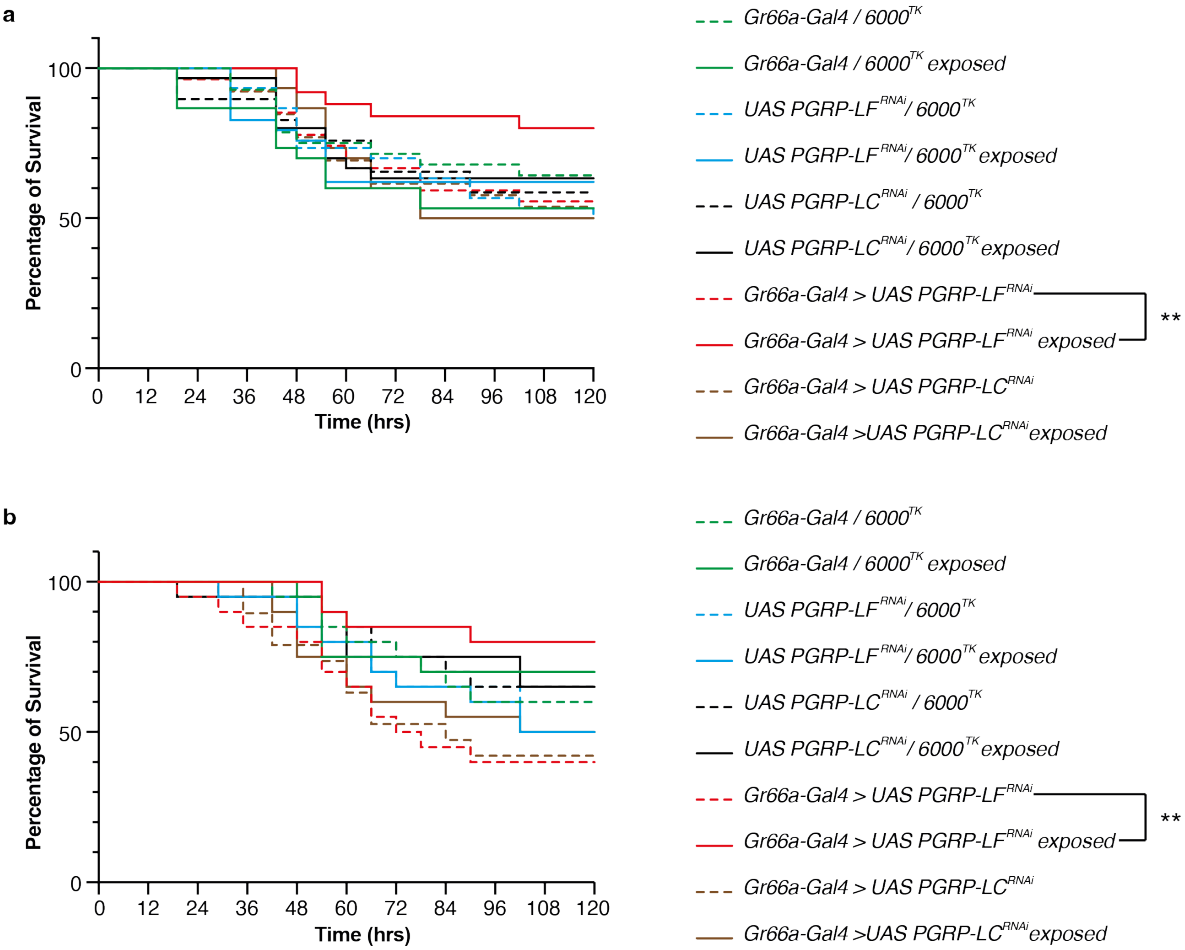

Extended Data Fig. 7. Overactivation of IMD pathway in Gr66a gustatory neurons primes the cellular immune pathway. Related to Fig. 7.

a, Schematic representation of the protocol for the exposition of germ-free larvae with *E. coli* followed by infection with *P. entomophila* in the adults. After oviposition the embryos are sterilized with bleach and transferred under sterile conditions into a vial containing ATB media. Then larvae are transferred to LB plates containing either *E.coli* or nothing for 30 minutes and placed back to LB media for 150 minutes. Then the larvae are placed on ATB media until adulthood.Adult flies are then infected by *P.entomophila* and their survival is monitored. **b**, Replicate of the survival experiment: Survival curves following infection with *P.entomophila* of flies previously exposed to *E.coli* (solid lines, *Gr66a-Gal4>6000*^{TK}, $n = 28$; *6000*^{TK}*/UAS-PGRP-LF*^{RNAi}, $n = 30$; *Gr66a-Gal4>UAS-PGRP-LF*^{RNAi}, $n = 27$; *6000*^{TK}*/UAS-PGRP-LC*^{RNAi}, $n = 29$; *Gr66a-Gal4>UAS-PGRP-C*^{RNAi}, $n = 26$) or to nothing (dashed lines, *Gr66a-Gal4>6000*^{TK}, $n = 30$; *6000*^{TK}*/UAS-PGRP-LF*^{RNAi}, n = 29; *Gr66a-Gal4>UAS-PGRP-LF*^{RNAi}, $n = 25$; *6000*^{TK}*/UAS-PGRP-LC*^{RNAi}, $n = 30$; *Gr66a-Gal4>UAS-PGRP-C*^{RNAi}, $n = 30$). **c**, Replicate of the survival experiment: Survival curves following infection with *P.entomophila* of flies previously exposed to *E.coli* (solid lines, *Gr66a-Gal4>6000*^{TK}, $n = 20$; *6000*^{TK}*/UAS-PGRP-LF*^{RNAi}, $n = 20$; *Gr66a-Gal4>UAS-PGRP-LF*^{RNAi}, $n = 20$); *6000*^{TK}*/UAS-PGRP-LC*^{RNAi}, $n = 20$; *Gr66a-Gal4>UAS-PGRP-C*^{RNAi}, $n = 20$) or to nothing (dashed lines, *Gr66a-Gal4>6000*^{TK}, $n = 20$; *6000*^{TK}*/UAS-PGRP-LF*^{RNAi}, $n = 19$; *Gr66a-Gal4>UAS-PGRP-LF*^{RNAi}, $n = 20$; *6000*^{TK}*/UAS-PGRP-LC*^{RNAi}, $n = 20$; *Gr66a-Gal4>UAS-PGRP-C*^{RNAi}, $n = 20$). Values represent mean. Statistical tests:one-sided log-rank test; $^{**}P < 0.01$.